

New insights into the star formation histories of candidate intermediate-age early-type galaxies from K' -band imaging of globular clusters

Iskren Y. Georgiev^{1*}, Paul Goudfrooij² and Thomas H. Puzia³

¹*Argelander Institut für Astronomie der Universität Bonn, Auf dem Hügel 71, D-53121 Bonn, Germany*

²*Space Telescope Science Institute, 3700 San Martin Drive, Baltimore, MD 21218, USA*

³*Department of Astronomy and Astrophysics, Pontificia Universidad Católica de Chile, Av. Vicuña Mackenna 4860, 7820436 Macul, Santiago, Chile*

Accepted 2011 November 1

ABSTRACT

We investigate the age and metallicity distributions of bright globular clusters (GCs) in the candidate intermediate-age early-type galaxies NGC 3610, NGC 584 and NGC 3377 using a combination of new Gemini/NIRI K' -band imaging and existing optical V, I photometry from Hubble Space Telescope data. The $V-I$ versus $I-K'$ colour-colour diagram is found to break the age-metallicity degeneracy present in optical colours and spectroscopy, as $I-K'$ primarily measures a populations' metallicity. In addition, it is relatively insensitive to the effect of hot horizontal branch (HB) stars that are known to be present in massive old GCs. By interpolation between Simple Stellar Population model tracks we derive photometric cluster ages, metallicities and masses. In general we find that "metal-poor" GCs with $[Z/H] \lesssim -0.7$ dex are older than more metal-rich GCs. For the most massive GCs ($M \geq 6 \times 10^5 M_\odot$) in NGC 3610 with available spectroscopic data, the photometric ages are older by ~ 2 Gyr, and this difference is more pronounced for the metal-poor GCs. However, the photometric and spectroscopic metallicities are in good agreement. We suggest that this indicates the presence of a hot HB in these massive clusters, which renders spectroscopic ages from Balmer line strengths to be underestimated. To support this suggestion we show that *all* Galactic GCs with $M \geq 6 \times 10^5 M_\odot$ feature hot HBs, except 47 Tuc. Using a recent observational relation between the luminosity of the most massive GC and the galaxy's SFR at a given age, we find that the galaxies' peak SFR was attained at the epoch of the formation of the oldest (metal-poor) GCs. The age and $[Z/H]$ distributions of the metal-rich GCs are broad, indicating prolonged galaxy star formation histories. The peak ages of the metal-rich GCs in the sample galaxies are 3.7, 5.9, and 8.9 Gyr for NGC 3610, NGC 584, and NGC 3377 respectively. The peak value of the age and metallicity distributions of the GCs is correlated with the host galaxies' luminosity-weighted age and metallicity, respectively, indicating that the GCs can indeed be used as relevant proxies of the star formation histories of galaxies.

Key words: galaxies: star clusters: general – galaxies: elliptical and lenticular, cD – galaxies: evolution – galaxies: formation – galaxies: individual (NGC 3610, NGC 584, NGC 3377)

1 INTRODUCTION

Globular clusters (GCs) are among the very few observable fossil records of the formation and evolution of galaxies. The nature of their integrated properties, closely approximated by a Simple Stellar Population (hereafter SSP), significantly simplifies the determination of their ages and metallicities

relative to that of the diffuse light of their parent galaxies. Hence they contain crucial information about the history of star formation and chemical enrichment of their parent galaxies (e.g., Whitmore et al. 1999; Goudfrooij et al. 2001). A key development in this respect has been the discovery that the GC systems of many early-type galaxies have bimodal colour distributions (e.g., Kundu & Whitmore 2001; Larsen et al. 2001; Peng et al. 2006), providing clear evidence for the occurrence of a "second event" in the for-

* E-mail: iskren@astro.uni-bonn.de

mation of these systems. Such a bimodal distribution was actually predicted from merger scenarios of E galaxy formation by Schweizer (1987); Ashman & Zepf (1992), who suggested that young GCs form out of chemically enriched gas during major gas-rich mergers, then redden and fade with time to produce the "red" population of GCs seen in old ellipticals. Since this prediction, populations of young and intermediate-age GCs have indeed been found in several gas-rich merger remnants (e.g. Holtzman et al. 1992; Schweizer et al. 1996; Miller et al. 1997; Whitmore et al. 1999; Goudfrooij et al. 2001 2001b; Goudfrooij et al. 2007).

Although HST studies have provided much information on the bimodality of GC systems, the typically used $V-I$ or $g-z$ colours provide only limited constraints on the age and metallicity of GCs. This is due to the well-known age-metallicity degeneracy, where increasing age or metal content have a similar effect in reddening the optical colours. The non linear relation between optical colour and metallicity adds an additional complication in the interpretation of colour bimodality (Yoon et al. 2006). In principle, spectroscopy is a more accurate way to estimate age and metallicity. However, in practice this is very time consuming even for an 8-10m class telescope, and only 1-2 handfuls of GCs per galaxy have been studied in this way to date with sufficient precision (e.g., Forbes et al. 2001; Goudfrooij et al. 2001; Puzia et al. 2005; Woodley et al. 2010; Alves-Brito et al. 2011).

Another way to break the age-metallicity degeneracy is to combine optical and near-infrared colours. In the optical, hot evolved stars (e.g., horizontal branch (HB) stars and blue stragglers) and young main sequence stars (if present) contribute significantly to the integrated light. They also enhance the strength of high-order Balmer lines, which causes a bias toward younger ages when classically derived from such absorption lines (see more in Sect. 5.1). Conversely, for ages > 1 Gyr, the near-IR is completely dominated by light from red giant stars. Thus near-IR colours like $I-K$ or $J-K$ measure the typical temperature of the giant branch, which is known to be directly sensitive to metallicity without any significant age dependence (e.g., Worthey et al. 1994). Relative to optical spectroscopy, the "optical+near-IR" imaging technique has the additional advantage that a larger number of GCs can be detected in a reasonable observing time per galaxy. This technique was pioneered for GCs in intermediate-age galaxies by Puzia et al. (2002) (see also Goudfrooij et al. 2001) using ground-based (ESO/VLT) K -band imaging in combination with Wide Field Planetary Camera 2 (WFPC2) V - and I -band data from *HST* to study NGC 3115 and NGC 4365, two nearby early-type galaxies. Puzia et al. (2002) found that NGC 4365 hosts a significant number of intermediate-age (2 – 6 Gyr old) GCs, whereas NGC 3115 only hosts "old" GCs. The age and metallicity values found for GCs by Puzia et al. (2002) were confirmed by subsequent spectroscopy of a handful of GCs in these two galaxies (Kuntschner et al. 2002; Larsen et al. 2003). Finally, the complications with the non-linear relation between optical colour and metallicity is safely avoided with optical-NIR colours (e.g. Cantiello & Blakeslee 2007; Kundu & Zepf 2007; Spitler et al. 2008). Hence, the optical+near-IR imaging technique is a valuable alternative to spectroscopy in studying GC age and metallicity distributions (see also Chies-Santos et al. 2011).

The discovery of a significant number of intermediate-age GCs in a fairly "normal" elliptical galaxies like NGC 4365 (Puzia et al. 2002, Kundu et al. 2005, but see Brodie et al. 2005, Chies-Santos et al. 2011) and NGC 5813 (Hempel et al. 2007a, 2007b) highlights the power of GCs in probing major star formation events in galaxies. While such an intermediate-age population in NGC 4365 might not seem unexpected given the presence of a kinematically decoupled core, it has not been identified from the galaxy's integrated light. This raises the important question whether or not early-type galaxies, which show signs of past interactions or mergers, generally host intermediate-age, metal-rich subpopulations.

In this paper we use the optical/near-IR technique mentioned above to constrain the presence of intermediate-age population(s) of GCs in a small sample of nearby early-type galaxies that show signs of having undergone a dissipative merger several Gyr ago. Our target galaxies are NGC 3610, NGC 3377 and NGC 584 described further in the next section.

2 THE TARGET GALAXIES

The target galaxies were selected to have the following properties at the time of proposal submission: (i) The galaxy is an E or E/S0 galaxy that is nearby enough ($v_{\text{hel}} < 2000 \text{ km s}^{-1}$) to detect several tens of GCs in the K band in reasonable exposure times, (ii) the galaxy has a rich GC system with *high-quality* optical GC colours measured with *HST* ($V-I$; Kundu & Whitmore 2001) whose distribution does not show a clear bimodality (the absence of such bimodality is expected in the presence of a significant subpopulation of GCs that is metal rich and of intermediate-age; see also Kissler-Patig et al. 1998), and (iii) measurement of (luminosity-weighted) age from integrated-light spectroscopy or photometry is in the range 2 – 5 Gyr. Table 1 lists relevant basic properties of the galaxies in our sample. Population properties of the sample galaxies from recent literature is discussed in more detail in Sect. 7.1).

3 OBSERVATIONS AND DATA REDUCTION

3.1 Observations

We performed near-infrared K' -band ($2.12 \mu\text{m}$) imaging of NGC 3610, NGC 3377, and NGC 584 with the Near-Infrared Imager and Spectrometer (NIRI) instrument on Gemini North (Hodapp et al. 2003). Our program ID was GN-2004A-Q-17. We used the f/6 NIRI camera imaging mode, which provides a plate scale of 0.117 arcsec/pixel and a field of view of $2 \times 2 \text{ arcmin}^2$, similar to the field of view of the WFPC2 and ACS cameras aboard *HST*.

In order to reliably detect the presence of both "blue" and "red" GCs, with $S/N \sim 5$ similar to that of the WFPC2 data, the targeted limiting magnitude was the typical turnover magnitude of GC systems of "normal" galaxies: $M_V = -7.3 \text{ mag}$ (e.g., Kundu & Whitmore 2001; Larsen et al. 2001), corresponding to $M_K = -9.8$ for a typical colour of an "old" (age of 14 Gyr) SSP with $[\text{Fe}/\text{H}] = -1.5$ (e.g. Bruzual & Charlot 2003). The exposure times to reach the limiting

Table 1. Basic properties of the sample galaxies.

Galaxy	Classification		A_V	$(m - M)_0$	D	M_V	$(V - I)_0$	$(I - K)_0$	Age_{spec}	$[Z/H]_{\text{spec}}$	SFR_{Peak}
	RSA	RC3	[Mag]	[Mag]	[Mpc]	[Mag]	[Mag]	[Mag]	[Gyr]	[dex]	$[M_{\odot}/\text{yr}]$
(1)	(2)	(3)	(4)	(5)	(6)	(7)	(8)	(9)	(10)	(11)	(12)
NGC 3610	E5	E5:	0.03	32.71 ± 0.08^c	34.84	-21.99	1.14	1.96	1.7 ± 0.1^e	$+0.76 \pm 0.16^e$	234
NGC 584	S0 ₁	E4	0.14	31.52 ± 0.20^a	20.14	-21.31	1.14	1.91	2.6 ± 0.3^d	$+0.46 \pm 0.03^d$	101
NGC 3377	E5-6	E6	0.11	30.17 ± 0.16^b	13.87	-20.01	1.11	1.81	3.7 ± 0.9^d	$+0.19 \pm 0.05^d$	75

Note. — Column descriptions: (1): Galaxy name. (2) and (3): Classification in RSA (Sandage & Tammann 1981) and RC3 (de Vaucouleurs et al. 1991) catalogs, respectively. (4): Foreground reddening in A_V according to (Schlegel et al. 1998). (5): Distance Modulus according to reference given (see below) and the corresponding distance in Mpc in (6) and galaxy absolute magnitude in (7). (8) and (9): $(V - I)_0$ and $(I - K)_0$ colours according to Michard (2005). (10) and (11): Spectroscopic age and $[Z/H]$ according to reference given (see below). (12): Galaxy peak SFR calculated in this study (see Sect. 7.2).

^aTonry et al. (2001); ^bHarris et al. (2007); ^cCantiello et al. (2007); ^dTrager et al. (2000); ^eHowell (2005).

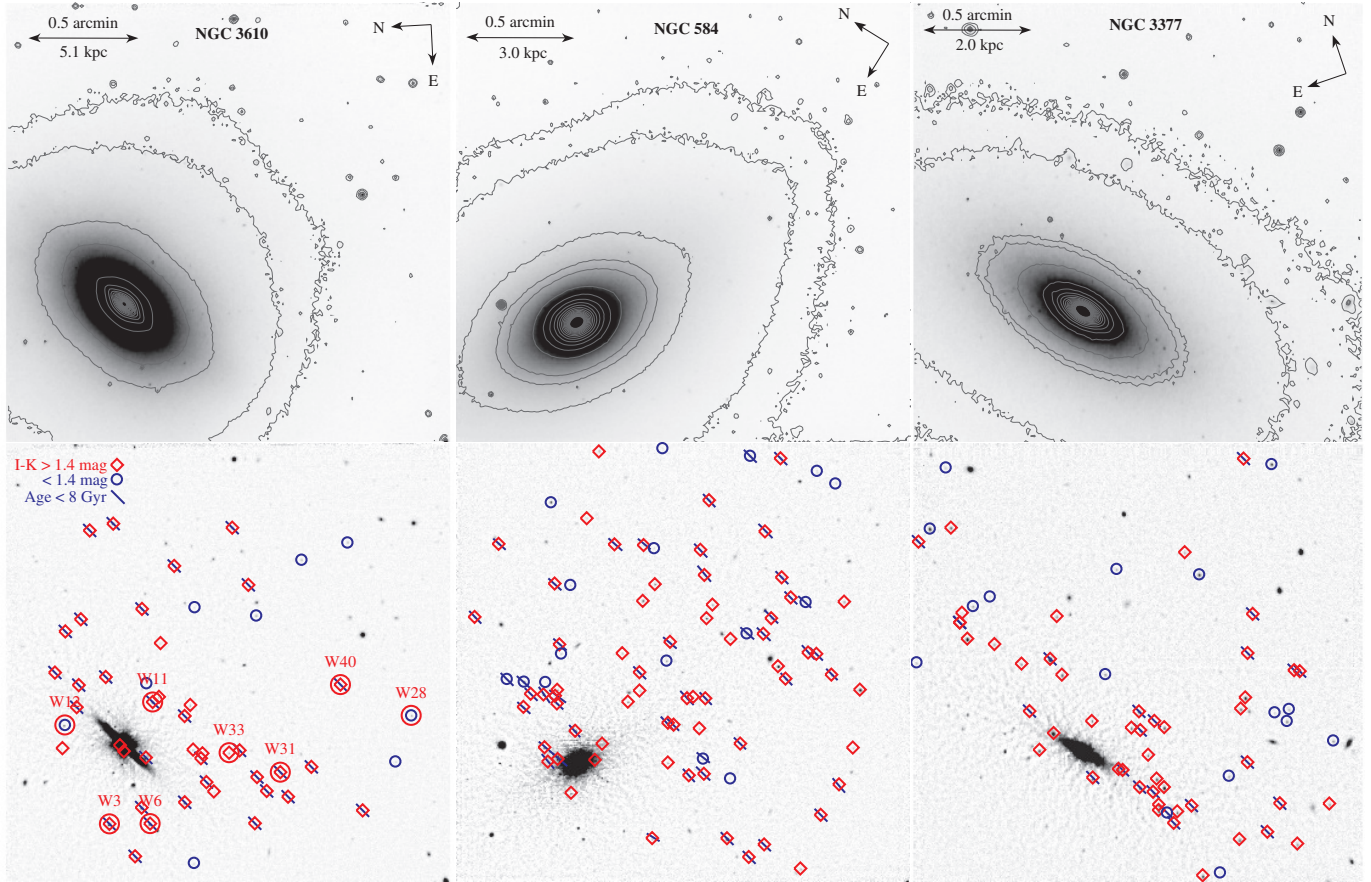


Figure 1. K' -band Gemini/NIRI images of NGC 3610, NGC 584 and NGC 3377 from left to right, respectively. The outer four isointensity contours on the top panels indicate surface brightnesses of $5, 10, 50$ and $100 \times \sigma$ above the background. Bottom panels show the galaxies with median filtered images subtracted. Different symbol types indicate globular clusters bluer (circles) or redder (diamonds) than $I - K = 1.4$ mag or younger than 8 Gyr (tilted solid line). NGC 3610 GCs with spectroscopic measurements in the literature are labeled and shown with larger circles.

magnitudes (cf. Table 2) were estimated according to the distance moduli and were such that NGC 3377 was observed in a single night, while NGC 3610 and NGC 584 required observations to be spread over two and four nights, respectively. Table 2 summarizes the observations and night conditions. In Figure 1 we show the spatial coverage of the NIRI ob-

servations. The character of the spatial distribution of detected GCs reflects the overlap between the NIRI and the HST/ACS/WFPC2 fields of view. Globular clusters shown with different symbols reflect their properties as derived in Section 5.

Table 2. Log of Observations

Target	Nights yyyy-mm-dd	FWHM arcsec	N images	Total Exposure seconds
NGC 3610	2004-02-10	0.43''	64	3840
	2004-02-11	0.35''	55	3300
NGC 584	2004-07-28	0.45''	35	2100
	2004-07-29	0.46''	34	2040
	2004-07-30	0.53''	31	1860
	2004-07-31	0.41''	38	2280
NGC 3377	2004-03-02	0.51''	28	1680

3.2 Data Reduction

Image reduction was performed with tasks of the GEMINI/NIRI¹ packages within IRAF². Due to the "first frame"³ problem of the NIRI detector, all first exposures (dark, flat and on-/off-target images) of each new sequence were excluded before basic image processing.

Normalized flats were constructed from images taken with the calibration unit shutter closed ("lamps off") subtracted from exposures taken with the shutter open ("lamps on") and using short darks to identify bad pixels. Flat field images with the IR lamp on and off allow separation of the instrumental thermal signature from the sensitivity response.

The near-IR sky level and structure varies on time scales of a few minutes. To account for such variations the imaging sequence of four on- followed by four off-target exposures provides close enough in time blank fields to derive the sky flat and correct the on-target exposures.

Some of the NIRI frames contain an electronic pattern visible as vertical striping with a period of eight columns and not always present in all quadrants. Before including the affected frames in our image processing list we used the stand-alone python routine, *nirinoise.py*⁴ which almost perfectly removed the striping. The same image reduction steps were applied to the standard star observations as well. We discarded few images which had trails or double-peaked stellar profiles reflecting the loss of the guide star resulting in improper telescope guiding.

All reduced science and standard star exposures of the corresponding nights were registered to a common coordinate system with NIRI/IMCOADD based on GEOMAP geometric solutions. The final science image of each galaxy is derived from average combined individual images scaled to that of the most photometric night for the case of NGC 3610

and NGC 584, which were observed over few nights. The total number of combined individual exposures for NGC 3610, NGC 3377, and NGC 584 is N=119, N=28, and N=137, respectively. The result is one deep stacked K' -band image per galaxy.

4 DETECTION, PHOTOMETRY AND CALIBRATION

4.1 Detection and photometry

Globular clusters in our ground based images would appear as unresolved point sources due to the relatively large NIRI pixel scale at the distances to the galaxies. For the nearest galaxy in our sample NGC 3377 at a distance of 10.8 Mpc we have a projected spatial resolution of 6 pc/pix. This is twice the typical half-light radius (~ 3 pc) of a GC (e.g. Barmby et al. 2007; Masters et al. 2010). NGC 3610 and NGC 584 are at much greater distances of 34.8 and 20.1 Mpc, respectively. Thus, even for the most nearby galaxy NGC 3377, the GCs on the ground-based images will appear as point sources with a stellar PSF, which determined the type of detection and photometry of GCs.

To detect⁵ as many GCs as possible to match with existing deeper HST photometry for these galaxies (Goudfrooij et al. 2007; Kundu & Whitmore 2001), we first created images representing the integrated light component of the galaxy by smoothing the combined images with a circular median filter with a radius of 8 times the seeing FWHM of the input image. The choice of the median filter radius resulted from tests designed to render the residual effect of point sources in the images negligible. This was done by measuring the magnitude difference between the original and median-subtracted images of several isolated non-saturated point sources. The original combined image was then divided by the square root of the smoothed image, providing an image with uniform shot noise characteristics (e.g., Goudfrooij et al. 2007). This facilitates the uniform detection of point sources at a detection threshold of 3σ above the background, using the DAOFIND task. The resulting object coordinates were used as input for PSF photometry performed on images from which the smooth galaxy light was subtracted. PSF models with radius $3 \times$ the point source FWHM were created using several non-saturated point sources. PSF-fitting magnitudes were scaled using aperture photometry with a radius of 4 pix for the PSF stars. To estimate aperture corrections from curve-of-growth analysis, photometry of the PSF stars was performed with aperture radii of $r = 2, 4, 12, 17, 21, 31$ pixels. We found very similar aperture corrections for the PSF magnitudes among the three sample galaxies (-0.361 ± 0.008 mag).

4.2 Photometric Calibration

Photometric calibration was performed using photometric standards (FS 6, FS 23, FS 34, FS 103, FS 111, FS 126, FS 130, FS 131 and FS 134) observed during the same nights as the target galaxies. Their instrumental magnitudes were

¹ <http://www.gemini.edu/sciops/data-and-results/processing-software>

² IRAF is distributed by the National Optical Astronomy Observatories, which are operated by the Association of Universities for Research in Astronomy, Inc., under cooperative agreement with the National Science Foundation.

³ First frame problem arises because the NIRI array is not continuously reset when idle. Thus, each new exposure after idle has different dark current level, probably due to image persistence after saturating the array (NIRI has no shutter).

⁴ <http://staff.gemini.edu/~astephens/niri/patternnoise/>

⁵ All reduction and analysis has been performed with IRAF procedures.

Table 3. Calibration Coefficients for Equation (1)

	$ZP_{K'}$	$c1^1$	$c2$
NGC 3610	-23.66 ± 0.03	0.07	-0.025 ± 0.024
NGC 584	-23.68 ± 0.04	0.07	-0.027 ± 0.021
NGC 3377	-23.68 ± 0.03	0.07	-0.026

measured with the same aperture as their measured K' catalog magnitudes in Leggett et al. (2006). Thus, we derive consistent transformation solutions from instrumental to standard photometric system for all objects in our photometric lists. To allow for optical-to-near-IR colour terms in the photometric calibration of the K' -band data, we used the V -band magnitudes of the photometric standard stars in Table 1 of Hawarden et al. (2001), who compiled measurements from Sandage & Katem (1982); Lasker et al. (1988); McCook & Sion (1987); Carlsberg Meridian Catalogue (1989); Leggett (1992); Landolt (1992). Hence, the derived photometric transformations will take into account the $V - K$ colour of the object.

We evaluated a least squares fit to the following photometric transformation equation:

$$mK' = K' + ZP_{K'} + c1 \times X_{K'} + c2 \times (V - K') \quad (1)$$

where mK' is the instrumental magnitude, $ZP_{K'}$ is the zero-point, $c1$ and $c2$ are the airmass and colour term coefficients. The zero-point and airmass coefficients were fitted around their typical values⁶ $ZP_{K'} = 23.68$ mag, $c1 = 0.059$ mag/airmass. However, a best fit (low rms and coefficients uncertainty) was achieved for fixed airmass coefficient at $c1 = 0.07$ mag/airmass⁷, while the zero-point and colour term coefficients were kept variable. This resulted in stable solutions for the zero-point and the $V - K$ colour term coefficients, close to their typical values (cf. Table 3). Due to the only one standard star observed during the NGC 3377 observing run, we fit the $ZP_{K'}$ using a constant value for the colour term, which is the mean value obtained from the NGC 3610 and NGC 584 calibrations. Excluding both, $c1$ and $c2$ from the fit results in a $ZP_{K'} = -23.73$ mag, i.e. within the uncertainty estimate of the $ZP_{K'}$ value with the airmass and colour coefficients included. All transformation coefficients are summarized in Table 3.

To convert the GCs' instrumental to standard K' magnitudes, V -band magnitudes of detected GCs in our images were adopted from the HST/ACS and WFPC2 optical V, I photometry in Kundu & Whitmore (2001) for NGC 584 and NGC 3377 and Goudfrooij et al. (2007) for NGC 3610. To match the NIRI and HST photometric lists, we transformed the ACS and WFPC2 GC pixel coordinates to the NIRI image pixel coordinate system by deriving geometric transformation solutions with GEOMAP and applying them with GEOXYTRAN IRAF routines. The transformation from instrumental to K' magnitudes of our sample GCs was performed by evaluating calibration equation (1), taking into account the $V - K'$ colour of the cluster. In Table 4 we list

the photometric properties of all GCs with K' photometry which are discussed in the following.

⁶ <http://www.gemini.edu/?q=node/10104>

⁷ The mean value found for a typical variation of the water vapor amount on Maunakea (Tokunaga et al. 2002)

Table 4. Magnitudes, colors, photometric age, metallicity and mass of globular clusters in the three post-merger remnant galaxies corrected for foreground reddening. Optical V , I magnitudes, coordinates and clusters IDs are from Goudfrooij et al. (2007) for NGC 3610 and Kundu & Whitmore (2001) for NGC 584 and NGC 3377. The second IDs for the NGC 3610 GCs are the IDs adopted in the spectroscopic study by Strader et al. (2003, 2004). Full version of this table is available online.

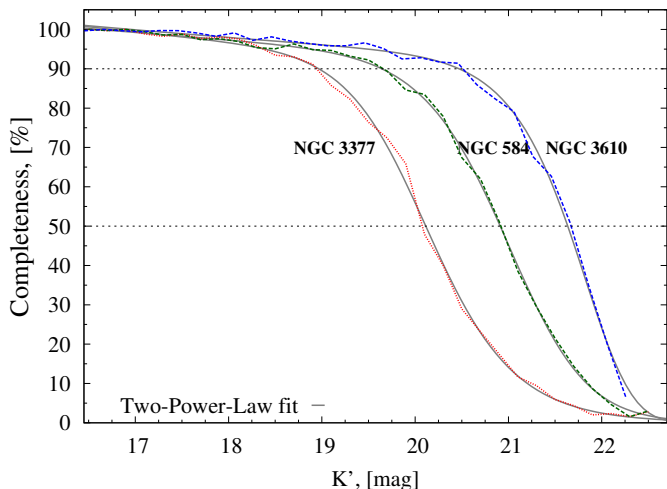


Figure 2. Completeness curves for object detection as a function of K' magnitude for the three studied galaxies. Dotted horizontal lines mark the 50% and 90% completeness limits shown in Table 5. Smooth solid lines show the two-power-law fit to the completeness distributions.

4.3 Completeness in K-band

To determine the completeness of the K-band observations, we used the ADDSTAR task in IRAF to add artificial sources to the final stacked image of each galaxy. To avoid introducing increased crowding to the images while retaining a high number of artificial stars per spatial and magnitude bin for reliable statistics, we added 100 stars per image and repeated this step 100 times⁸, i.e. in total 10^4 artificial stars per galaxy. The images were then run through the same extended galaxy light subtraction, detection and photometry steps. Detected and input artificial star lists were matched to compute the completeness as a function of K' magnitude. The completeness curves are shown in Figure 2. With smooth solid lines we show a two-power-law fit to the completeness values at each 0.5 mag bin. These functions were later used to assess completeness levels as a function of age and metallicity (see Sect. 5.3)

In Table 5 we summarize the 50% and 90% completeness values for the three galaxies. The absolute V -band magnitude (M_V) was calculated using the galaxies' respective distance moduli (see Sect. 3.1), and a $V - K' = 2.5$ mag colour for the GCs, which is the mean of the observed range of $2.0 \lesssim V - K' \lesssim 3.0$ mag. Thus, at the respective distance to these galaxies we observe, with 50% completeness, just at the GC luminosity function turnover magnitude (GCLF ToM) for NGC 3377, and about 0.5 and 1 mag brighter than the GCLF ToM for NGC 584 and NGC 3610, respectively. This corresponds to a luminosities greater than a few $10^5 L_\odot$, meaning that our K' -band GC detection samples the brightest and most luminous GCs. We note, that the currently best estimate of the distance modulus of NGC 3610 was derived ~ 3 yrs after the observations (see Sect. 3.1), which were planned with a closer distance to NGC 3610. This led to a lower completeness than planned for NGC 3610.

Table 5. Completeness limits for object detection from K' -band completeness test. M_V calculated using a mean $V - K' = 2.5$ mag colour.

Target	K' [mag]	M_V [mag]	L_V [$10^5 L_{V,\odot}$]
50% completeness			
NGC 3610	21.71	-8.50	2.1
NGC 584	20.92	-8.12	1.5
NGC 3377	20.08	-7.59	0.92
90% completeness			
NGC 3610	20.51	-9.70	6.4
NGC 584	19.66	-9.36	4.7
NGC 3377	18.95	-8.72	2.6

5 VIK' COLOUR, AGE AND METALLICITY DISTRIBUTIONS OF GCS

As already mentioned in the Introduction, the combination of optical and near-infrared imaging photometry is a very efficient method to access the distribution of ages and metallicities for an entire globular cluster system of a galaxy by means of a comparison to predictions of stellar population synthesis models. The specific power of this "optical+NIR" method is twofold:

- (i) for a population of coeval stars older than $\gtrsim 1$ Gyr, near-IR colour indices like $I - K$ or $J - K$ mainly sample the metallicity sensitive temperature distribution of stars on the RGB (e.g. Worthey 1994). In combination with an optical colour like $V - I$, which is sensitive to both metallicity and age, this allows to break down the age-metallicity degeneracy present in the optical colour indices.
- (ii) Relative to optical colours and spectral indices, near-IR colours are significantly less sensitive to the presence of *evolved* hot stars such as blue horizontal branch (HB) stars and blue stragglers. Blue HBs can be present in GCs older than ~ 8 Gyr (starting with metal-poor GCs; see e.g. Lee et al. 2000; Yi 2003), and the relative number of blue versus red HB stars in GCs is known to depend mainly on age, metallicity, and GC mass (e.g., Carretta et al. 2010; Dotter et al. 2010, 2011). Hence, the presence of blue HB stars in GCs can cause incorrect age determinations when using optical photometry or spectroscopy (see also Schiavon et al. 2004; Cenarro et al. 2007; Percival & Salaris 2011), while NIR colours are largely insensitive to their presence.

In the following, our age-metallicity analysis will be based on $V - I$ versus $I - K'$ diagrams.

In Figure 3, we present the $V - I$ vs. $I - K'$ colour-colour distributions of all GCs detected in K' in our sample galaxies. Those are compared to Bruzual & Charlot (2003) SSP models using a canonical Chabrier (2003) IMF, for several ages (1, 2, 5, and 14 Gyr) and metallicity values ($Z/Z_\odot = 0.005, 0.02, 0.2, 0.4, 1.0$, and 2.5, equivalent to $[\text{Fe}/\text{H}] = -2.3, -1.7, -0.7, -0.4, 0.0$, and $+0.4$)⁹. Figure 3 shows

⁸ The value of the seed in ADDSTAR was different for each frame

⁹ We note that the quoted photometric $[\text{Fe}/\text{H}]$ is in fact $[\text{Z}/\text{H}]$, i.e. the total content of metals relative to hydrogen given in the SSP models. However, the difference between $[\text{Z}/\text{H}]$ and $[\text{Fe}/\text{H}]$ is $0.03 \text{ dex} < \Delta[\text{Fe}/\text{H}] < 0.06 \text{ dex}$ for low to high metallicities, i.e.

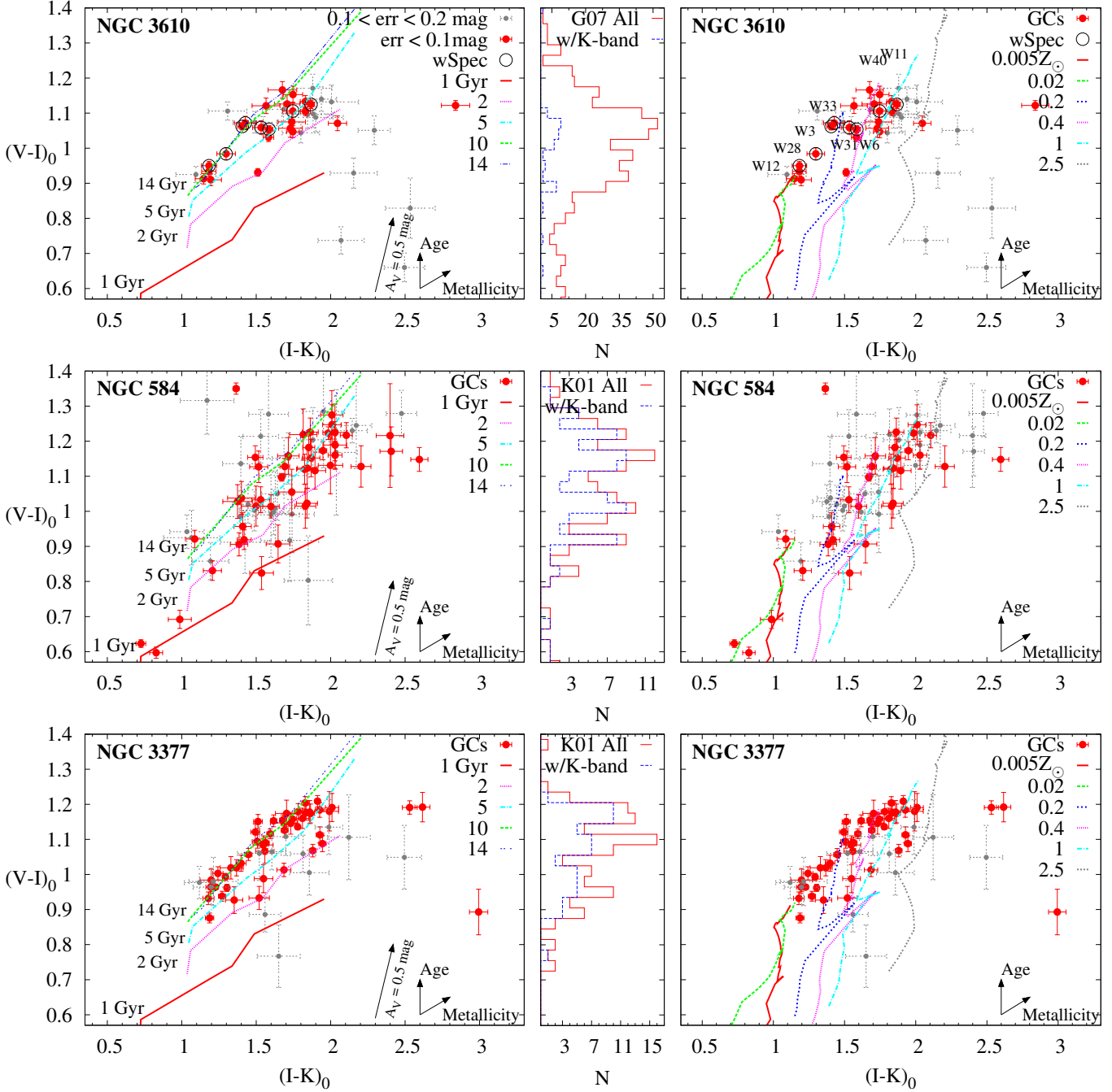


Figure 3. Optical-NIR $(V-I)_0$ vs. $(I-K)_0$ colour-colour distributions of globular clusters (solid circles) in NGC 3610, 584 and 3377 from top to bottom, respectively. Encircled solid symbols mark GCs with spectroscopic measurements in NGC 3610 (Strader et al. 2003, 2004). Small dots are GCs with colour error greater than 0.1 mag. colour indices are foreground reddening corrected. **Middle panels** show histograms of $(V-I)_0$ colour distributions of the GC population detected with HST (with solid line) and those with NIRI K' -band magnitudes (dashed line). Smaller solid circles with dashed line error bars show GCs with colour uncertainty larger than 0.1 mag. **Left and right panels** show a comparison between cluster colours and expectations for ages and metallicities from Simple Stellar Population (SSP) synthesis models (Bruzual & Charlot 2003). Different line-types indicate isochrones of different ages for all metallicities covered by the models (left panels) and isometallicity SSP tracks for ages > 0.5 Gyr (right panels). The arrows in the bottom panels show the direction of increasing age and metallicity, as well as a reddening vector for $A_V = 0.5$ mag.

much smaller than the measurement error. To avoid confusion in the following we adopt the $[\text{Fe}/\text{H}]$ annotation for the photometric metallicities as well.

that the three galaxies generally show a large spread in age and metallicity among their brightest GCs. A notable subpopulation of roughly coeval bright GCs can be also seen for NGC 3377 (see below). The $I-K'$ colours of the majority of the "blue" population of GCs as judged from the

optical data (i.e., $V - I < 1.0$) turn out to be consistent with old ages ($\gtrsim 5$ Gyr) and low-metallicities on average ($-2.3 \lesssim [\text{Fe}/\text{H}] \lesssim -0.7$ dex), while the $I - K'$ colours of the optically redder clusters tend to indicate higher metallicities and younger ages ($[\text{Fe}/\text{H}] \gtrsim -0.7$ dex and $\sim 3 - 6$ Gyr, respectively).

While the overall colour-colour distributions are indicative of a large spread in age and metallicity among the brightest clusters, there is a discernible population of roughly coeval GCs in NGC 3377 (i.e., the GCs between the 2 and 5 Gyr isochrones in the lower left panel of Fig. 3). From our data alone, there is no indication for a spatial correlation among these clusters (cf Fig. 1). While such a subpopulation is not readily seen in the other two galaxies, this may be due at least in part to the photometric completeness limits (cf. Table 5). The middle panel histograms in Figure 3 show that our NIRI imaging detects 61% (64/106), 73% (81/115) and 8% (50/611) of the NGC 3377, NGC 584 and NGC 3610 GCs detected with HST, respectively. Although the NIRI imaging samples 73% of the NGC 584 GCs observed with WFPC2, the relatively large photometric errors cause a larger scatter in their VIK' colour distributions, which prohibits a clear detection of any underlying subpopulation of coeval GCs similar to that observed in NGC 3377.

5.1 Photometric ages and metallicities

Employing the good resolution in age and metallicity provided by the optical-NIR (V, I, K) colour indices, we derive photometric ages and metallicities for the GCs in our sample. This is done by a standard χ^2 minimization interpolation between SSP model tracks of Bruzual & Charlot (2003). A brief comparison with other SSP models and the reasoning why we chose Bruzual & Charlot models for this purpose is presented in Section 5.2. The derived ages and metallicities are the weighted average of the age and metallicity of the two nearest tracks. The weights include the distance to the respective model and the photometric errors. This way we also calculate an upper and lower error to the photometric ages and metallicities. We list the derived properties of all GCs in our sample in Table 4.

About a dozen of the brightest GCs in NGC 3610 have available Lick index analysis of optical spectroscopy (Strader et al. 2003, 2004). Strader et al. qualitatively discuss the clusters ages, but they do not explicitly provide ages for each cluster. Thus, using their Lick index strengths, we calculate ages for the GCs with the GONZO code (Puzia et al. 2002), using the models of Thomas et al. (2003). Of those GCs, eight are within the NIRI field of view for which we can compare our ages and metallicities with their spectroscopic values. In Figure 4 we show these differences (in the sense spectroscopic minus photometric) as a function of $I - K'$ colour. Errors in the top and middle panels in Figure 4 are the square root of the sum of the squares of the spectroscopic and photometric errors while errors in the bottom panel are their photometric uncertainties.

The least squares fit to the data (dashed lines in Fig. 4) show that spectroscopic $[\text{Fe}/\text{H}]$ and photometric metallicities $[Z/\text{H}]$ derived from the VIK colours agree very well, keeping in mind that $[\text{Fe}/\text{H}] - [Z/\text{H}] = 0.03$ to 0.06 dex (cf. Sect. 5 above). In contrast, the photometric age estimates of the most massive GCs in NGC 3610 are older than their

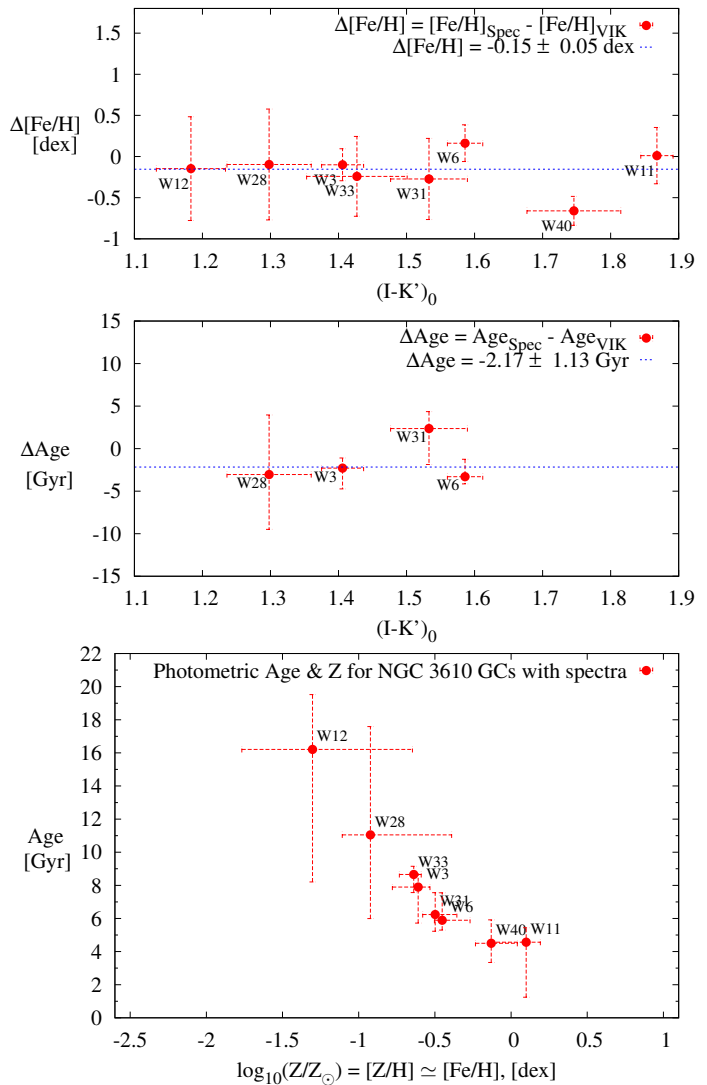


Figure 4. Differences between spectroscopic and photometric metallicities (**top**) and ages (**middle**) for NGC 3610 GCs. Dashed lines are the least squares fit. **Bottom** panel: photometric ages and metallicities for NGC 3610 GCs with spectra. The top panel shows that VIK derived metallicities are well consistent with their spectroscopic values. On average, photometric ages are older than spectroscopic ones by ~ 2 Gyr (middle panel), and the difference between them is more pronounced for low-metallicity GCs than those with higher Z s, possibly due to the presence of blue horizontal branch (see text in Sect. 5.1).

spectroscopic values by about 2 Gyr on average. The age difference is larger for low-metallicity GCs than for higher metallicity ones. Such a difference can in principle be caused by the presence of blue horizontal branch (BHB), helium-core burning stars in these clusters. It is well known that spectroscopic luminosity-weighted ages, derived from the classical H_{β} vs $\text{Mg}2$ or Mgb absorption line indices, can be biased toward younger ages, especially for metal-poor GCs, because the high effective temperature of BHB stars ($T_{\text{eff}} > 9000$ K) and blue stragglers enhances the strength of the Balmer lines (e.g. Lee et al. 2000; Schiavon et al. 2004; Koleva et al. 2008; Ocvirk 2010; Percival & Salaris 2011; Xin et al. 2011). An example for such "age bias" are the metal-poor Galactic GCs NGC 3201 and NGC 5024 featur-

ing BHBs, whose spectroscopically derived age (from H_β vs. Mg_2) is ~ 8 Gyr (Perina et al. 2011), while their ages from deep HST CMD fitting is $\gtrsim 12$ Gyr (Dotter et al. 2010). Furthermore, nearly all massive ($M \gtrsim 3 \times 10^5 M_\odot$, $M_V < -8.9$ mag) Galactic GC have hot HBs (e.g. Recio-Blanco et al. 2006; Lee et al. 2007), with the exception of the metal-rich GC 47 Tuc. This may be due to its low central escape velocity (v_{esc}) for a massive cluster at that metallicity, unlike the metal-rich NGC 6388 and NGC 6441 which do have BHBs and larger v_{esc} (cf. Fig. 5 in Georgiev et al. 2009) and thus better able to retain/accrete processed stellar ejecta. Puzia et al. (2002) performed a Lick index analysis for metal-rich Galactic GCs and they note that NGC 6388 and NGC 6441 (which host BHB stars) show a stronger H_β index than the other metal-rich RHB GCs. However, Schiavon et al. (2004) estimate ages of ~ 8 and ~ 11 Gyr from Lick index spectroscopy for these two clusters, which indicates that spectroscopic age-dating of metal-rich GCs can be less biased by the HB morphology. This is what we do indeed observe in the middle panel of Figure 4 for W 6 and W 31, two metal-rich GCs in NGC 3610: their photometric and spectroscopic ages are more consistent (see also Sect. 6). More pronounced HB effect is expected for metal-poor GCs, which we indeed observe for the two metal-poor GCs in the middle panel of Figure 4. This indicates that in spite of uncertainties inherent to SSP models, the most likely cause for the mean difference between photometric and spectroscopic ages for these GCs is the presence of hot HB stars, in particular for the metal-poor GCs.

The validity of the method of deriving ages and metallicities from V , I , and K photometry used in this paper is supported by the observation that dereddened $V-I$ and $V-K$ colours of old GCs in the Milky Way and M31 have been shown to be consistent with Bruzual & Charlot SSP model predictions for "old" ages ($\gtrsim 10$ Gyr) throughout the range of $[Z/H]$ sampled, (see Fig. 5 of Puzia et al. 2002). The applicability of our method is illustrated in Figure 5 using the same M31 GCs data as in Puzia et al. (2002), i.e. V , I magnitudes from Barmby et al. (2000, 2001), augmented with new spectroscopic measurements from Beasley et al. (2005) and Caldwell et al. (2011), the latter providing updated $E(B-V)$ values. Even though the $E(B-V)$ are uncertain ($\sigma \sim 0.1$ mag, see Caldwell et al. 2011), the $V-I$, $I-K$ colours are consistent with the Bruzual & Charlot SSP model predictions, even so for GCs massive ($M > 6 \times 10^5 M_\odot$) and $E(B-V) < 0.3$ mag. We derive their photometric ages and metallicities, which compare well with their spectroscopic values from Caldwell et al. (2011), while spectroscopic ages for the oldest GCs ($\text{Age}_{\text{VIK}} > 8$ Gyr), on average, are younger, i.e. showing the BHB effect. Due to this problem, Caldwell et al. (2011) does not derive spectroscopic ages for the majority of the GCs and assume age of 14 Gyr. We consider only GCs with spectroscopic ages in Figure 5.

5.2 Comparison to various SSP models

It is beyond the aims of this paper to test different SSP models and investigate the nature of the differences between them. However, in order to provide a qualitative overview of how different synthesis population models compare to the observed colours of NGC 3610 GCs with available spectroscopy, we compare our data with the popular SSP models

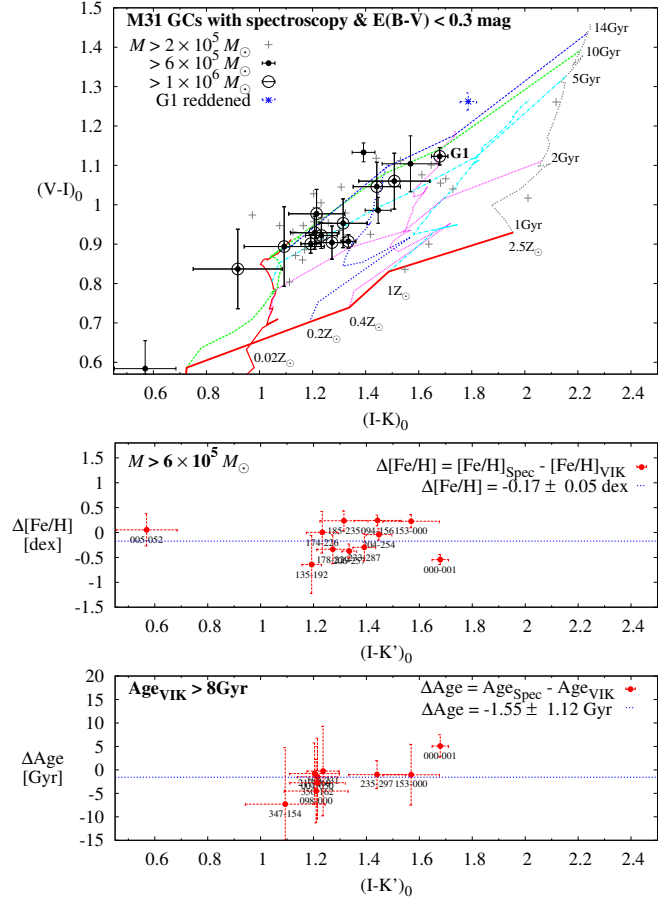


Figure 5. Comparison between VIK photometric and spectroscopic ages and metallicities for M31 GCs. **Top:** Brightest (most massive) and less reddened ($E(B-V) < 0.3$ mag) M31 GCs, as indicated in the legend, which we consider having the most reliable photometric and spectroscopic measurements. VIK magnitudes are from Barmby et al. (2000, 2001) and spectroscopic ages and metallicities from Beasley et al. (2005) and Caldwell et al. (2011). Colours were dereddened using $E(B-V)$ values from these studies. In spite of the large photometric and reddening uncertainties, we derive similar photometric and spectroscopic metallicities (**middle panel**), while spectroscopic ages for the oldest GCs ($\text{Age}_{\text{VIK}} > 8$ Gyr) are younger on average (**bottom panel**), signaling the BHB effect. In both panels, dashed horizontal lines are the least-squares fits to the data, with coefficients shown in the legend.

of BC03 (Bruzual & Charlot 2003), Gaev (Anders & Fritzev. Alvensleben 2003; Anders et al. 2009), Vazdekis/MILES (Vazdekis et al. 2010), TSPoT (Brocato et al. 2000; Raimondo et al. 2005), and the Maraston (Maraston 2005) SSPs for blue and intermediate-to-red HBs. Results are shown in Figure 6. As seen, the different SSP models yield significantly different results in terms of ages and metallicities. This is due in part to the different treatment of key stellar evolutionary phases, e.g. the TP-AGB and post-AGB phases, HB stars, etc., which are relatively poorly understood and empirically constrained. In addition, the different SSP models use different stellar atmosphere spectral libraries (theoretical or empirical), and different stellar evolution prescriptions. The effects of different choices of the IMF on the integrated VIK' colours are, however, smaller than the observational errors.

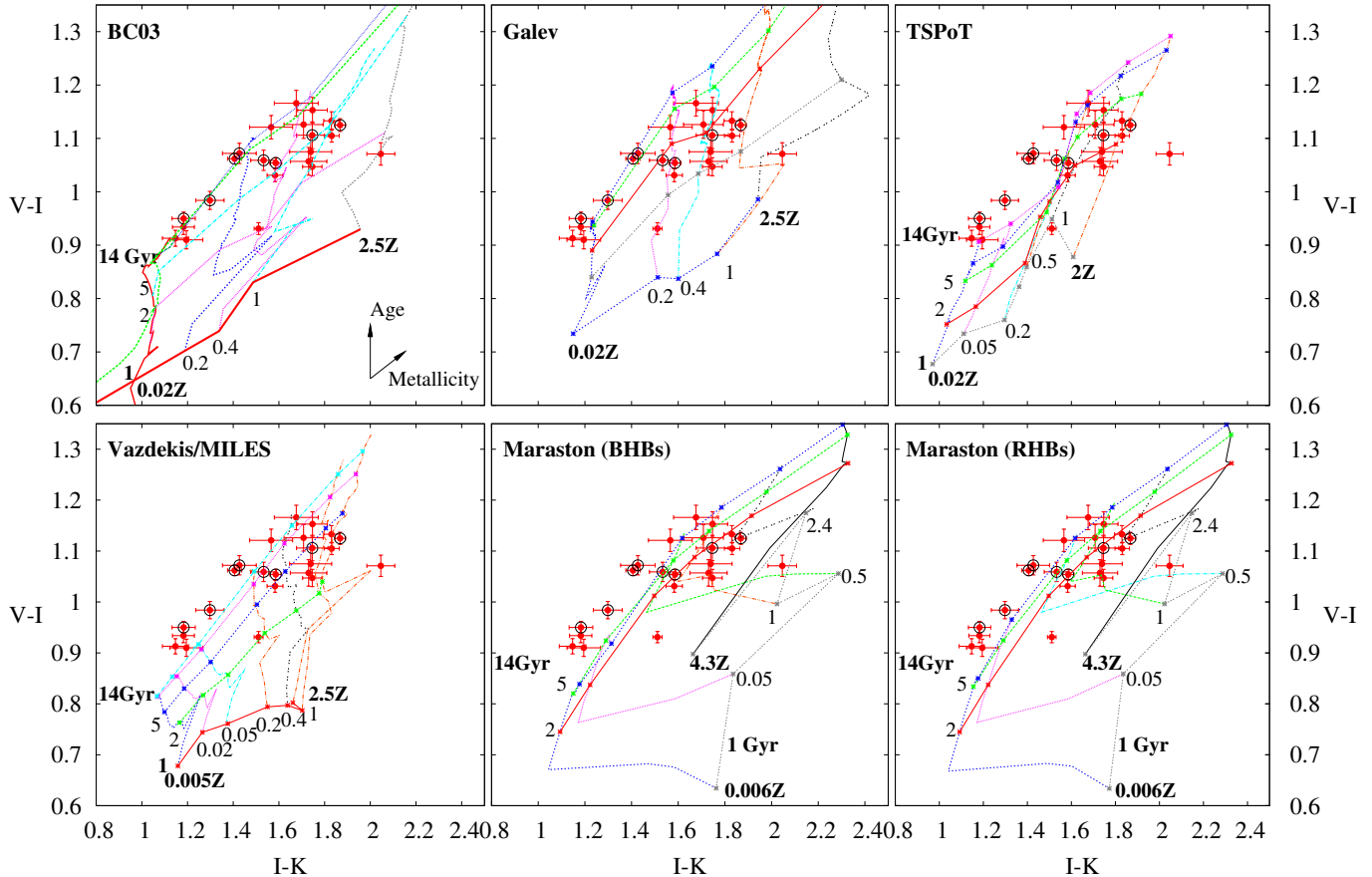


Figure 6. Comparison between $V - I, I - K'$ colours of GCs in NGC 3610 with colour errors < 0.1 mag and different SSP synthesis models (see text in Sect. 5.2). With circles are GCs which have spectroscopically derived ages and metallicities. In the top left panel with arrows are indicated the direction of increasing age and metallicity. With labels are indicated the 1, 2, 5 and 14 Gyr isochrones and isometallicity SSP tracks with labeled values. All models are with canonical IMF (Kroupa 2001; Chabrier 2003). MILES SSPs are with the revised Kroupa IMF, which accounts for effects from unresolved binaries. Only Bruzual & Charlot SSP models provide K' magnitudes, however, the $K - K'$ difference is from -0.02 to 0.007 mag for high to low metallicities, respectively, which is negligible to account for differences between data and models. The Maraston models include the blue and intermediate-red horizontal branches tracks, which differ for ages > 5 Gyrs.

Overall, our VIK' data is best represented by the BC03 SSP model, especially for low metallicities and old ages. This is why we use BC03 to derive and discuss ages and metallicities for our clusters in the following.

5.3 GC age and metallicity distributions

In Figure 7 we show the VIK' photometric age and metallicity distributions for the GCs in the three target galaxies. Employing the good separation in the $I - K$ colour in the SSP models (cf e.g. Fig. 3) between metal-rich and metal-poor and older versus younger populations, we separate the GCs in two subpopulations, namely redder and bluer than $I - K = 1.4$ mag, corresponding to $[Z/H] \sim -1$ dex for a population older than about 5 Gyr. Within R^{10} , we then estimate the highest-probability age for the metal-rich GCs using a non-parametric probability density estimator with a

Gaussian kernel with size of 2 Gyr. Those probability density estimates are shown with solid lines in Figure 7 and the peak values for the age distribution of the metal-rich GCs (Age_{red}) are shown with labels. It is seen that Age_{red} increases from ~ 4 Gyr for NGC 3610, to ~ 6 Gyr for NGC 584 and ~ 9 Gyr for NGC 3377. To assess the statistical level of similarity between the age distributions of the three galaxies, we consider that one can not expect Gaussian (or any other anticipated functional form) for the cluster age distributions. Formally, this precludes the use of the Kolmogorov-Smirnov test which is commonly used for comparing statistical similarity between two samples. We therefore use the Mann-Whitney U test¹¹, which yields that the distribution of GC ages in NGC 3610 is different from those of NGC 584 and NGC 3377 with a probability of 75% and 98%, respec-

¹⁰ R is a language and environment for statistical computing and graphics (<http://www.r-project.org>).

¹¹ The Mann-Whitney U test (a.k.a. Mann-Whitney-Wilcoxon rank-sum test or u-test) is a *non-parametric* statistical hypothesis test which calculates a measure of the difference between two *independent* samples of observations. It is similar to the t-test, but is more robust because it compares the sums of ranks and thus is less sensitive to the presence of outliers.

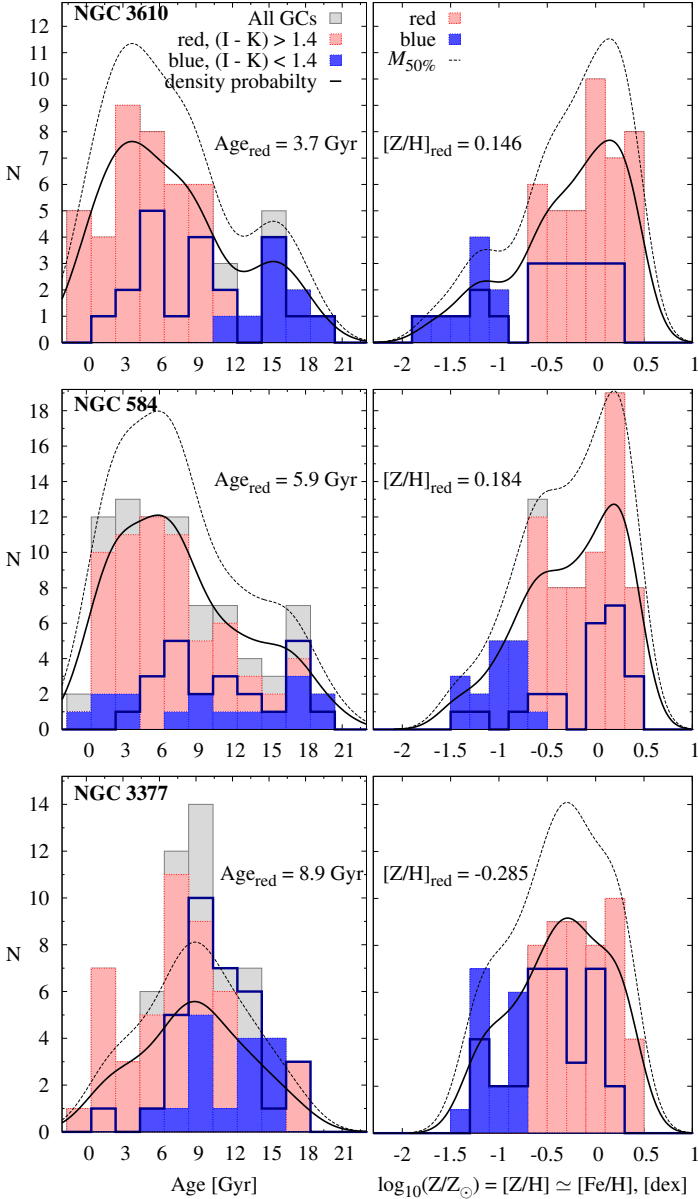


Figure 7. *VIK* photometric age and metallicity distributions (left and right panels) for all GCs in the three post-merger remnant galaxies, i.e. NGC 3610, NGC 584 and NGC 3377, from top to bottom respectively. Light solid (gray), solid (red) and dark solid (blue) histograms show all GCs, redder and bluer than $I - K' = 1.4$ mag, respectively. Solid lines show the probability density distribution for all GCs. The highest probability density age for the red, metal-rich GCs, shown with label for each galaxy, increases from top to bottom. Dashed lines indicate the number density distribution corrected for 50% incompleteness (details in text in Sect. 5.3). Open solid line histograms present GCs with mass larger than the mass at 50% incompleteness at 14 Gyrs (cf. also Fig. 9).

tively. The age distribution of GCs in NGC 584 differs from that in NGC 3377 with 98% probability. Thus, the brightest GCs in NGC 3610, NGC 584 and NGC 3377 have statistically significant different age distributions from one another and the peak age of the metal-rich subpopulation increases from NGC 3610 to NGC 584 and NGC 3377, respectively. The age and metallicity distributions are affected by

observational incompleteness. To assess the correction that likely needs to be applied, we used the functional relations between K' , mass, Z and Age using the Bruzual & Charlot (2003) SSP model. Since the HST/ACS and WFPC2 V, I -band photometry is 100% complete for all K' detections, no additional V, I completeness corrections are necessary. We fit power-law and logarithmic functions to the K' vs. $[\text{Fe}/\text{H}]$ and age relations for mass at the 50% completeness level at 2 and 14 Gyr and for all metallicities, respectively, obtained from the Bruzual & Charlot (2003) SSP models (cf. lines in Fig. 9). The age and $[\text{Fe}/\text{H}]$ distributions were then convolved with these functional relations to illustrate the completeness correction for 50% incompleteness. These estimates are shown with light dashed lines in Figure 7. Due to the relatively shallow slope of the $M - Z$ relation (cf. Fig. 9), the incompleteness affects equally metal-poor and metal-rich GCs, unless if metal-poor GCs tend to be larger and less dense which could bias their detection.

Keeping in mind photometric uncertainties, the age and metallicity distributions in Figure 7 seem to indicate the presence of multiple GC populations in the sample galaxies.

6 COLOUR-MAGNITUDE AND MASS-METALLICITY DISTRIBUTIONS

The colour-magnitude diagrams of GCs in the three merger-remnant galaxies is presented in Figure 8. With different lines in the left-hand panels of Figure 8 we show Bruzual & Charlot (2003) SSP model tracks for all metallicities scaled to the luminosity of a GC with $\mathcal{M} = 10^6 M_\odot$ at 14 Gyr, using model M/L_V values. The iso-mass lines in the right-hand panels in Figure 8 are calculated using the model M/L_V at 14 Gyr. This comparison shows that the masses of the GCs with K' data range from a few $10^5 M_\odot$ up to a few $10^6 M_\odot$. The upper and lower solid lines in the left panels labeled with 50% completeness indicate the 50% completeness at 14 and 2 Gyr, respectively, estimated using the SSP model prediction for the $I - K$ colour.

To convert the colour-magnitude diagrams to mass-metallicity distributions, we use M/L_V values provided by the SSP model to convert from GC luminosities to masses using the distance moduli to the galaxies. For comparison purposes, we also include info on GCs in the Milky Way (hereafter MW GCs). MW GC masses were calculated using data from McLaughlin & van der Marel (2005) and Harris (1996). In Figure 9 we show the mass-metallicity distributions of all GCs in the sample galaxies. To highlight the GCs that are old enough to have developed HBs, we divide the GCs in two subsamples: older or younger than 8 Gyr (solid blue circles and open red squares, respectively). The MW GCs with extended¹² HBs, i.e. EHBs, blue HBs, or red HBs in the bottom panel are shown with solid (blue) circles, (blue) crosses and open (red) squares, respectively. As Figure 9 shows, all MW GCs more massive than $6 \times 10^5 M_\odot$ (indicated with a horizontal dashed line) have hot HBs (EHBs or BHBs), except 47 Tuc.

As expected, the GCs in NGC 3610 with spectroscopy

¹² $\Delta V_{\text{HB}} > 3.5$ mag; Lee et al. (2007).

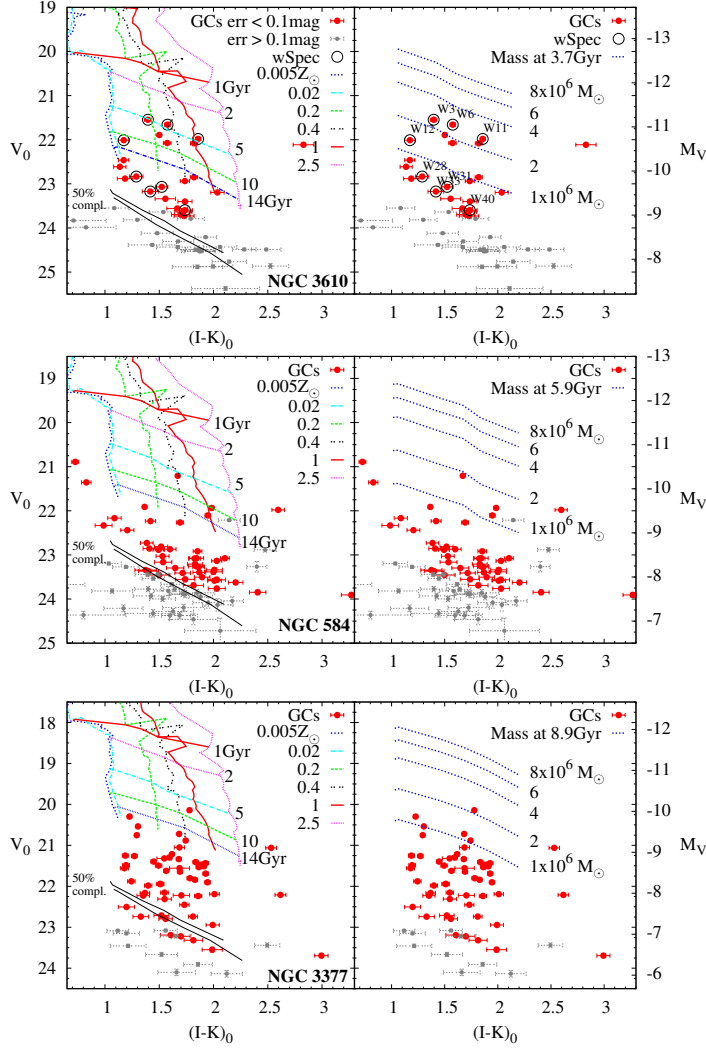


Figure 8. Colour-magnitude distribution of GCs (solid circles) in NGC 3610, 584 and 3377, from top to bottom, respectively. Large circles are GCs with colour error < 0.1 mag. With circles in the NGC 3610 panels are indicated GCs with spectroscopic observations in the literature (Strader et al. 2003, 2004). Lines in the **left panels** show 1, 2, 5, 10 and 14 Gyr isochrones and isometallicity Bruzual & Charlot (2003) tracks for $10^6 M_{\odot}$ and Z indicated in the legend. Lines in the **right panels** mark a constant mass for all metallicities at GCs' peak age obtained from the probability density distributions in Fig. 7, using the M/L_V -ratios provided in the models. The upper and lower solid lines in the left panels labeled with 50% completeness indicate the 50% completeness at 14 and 2 Gyr.

are among the most massive ones ($M > 6 \times 10^5 M_{\odot}$). However, among those, only W28 is formally older than 8 Gyr with $t = 11.047^{+6.541}_{-2.2}$ Gyr, and the age of W3 is $t = 7.9^{+0.8}_{-0.6}$ Gyr, equal to 8 Gyr within the measurement errors. This renders them good candidates for GCs that host BHB stars. This further supports the interpretation of the difference between photometric and spectroscopic ages due to the effect of the BHB in these metal-poor GCs as discussed in Section 5.1. On the other hand, the younger W31 and W6 ($t = 6.3^{+1.3}_{-1.0}$ Gyr, $[Z/H] = -0.498 \pm 0.082$ and $t = 5.9^{+1.8}_{-0.6}$ Gyr, $[Z/H] = -0.610 \pm 0.169$) likely have not yet

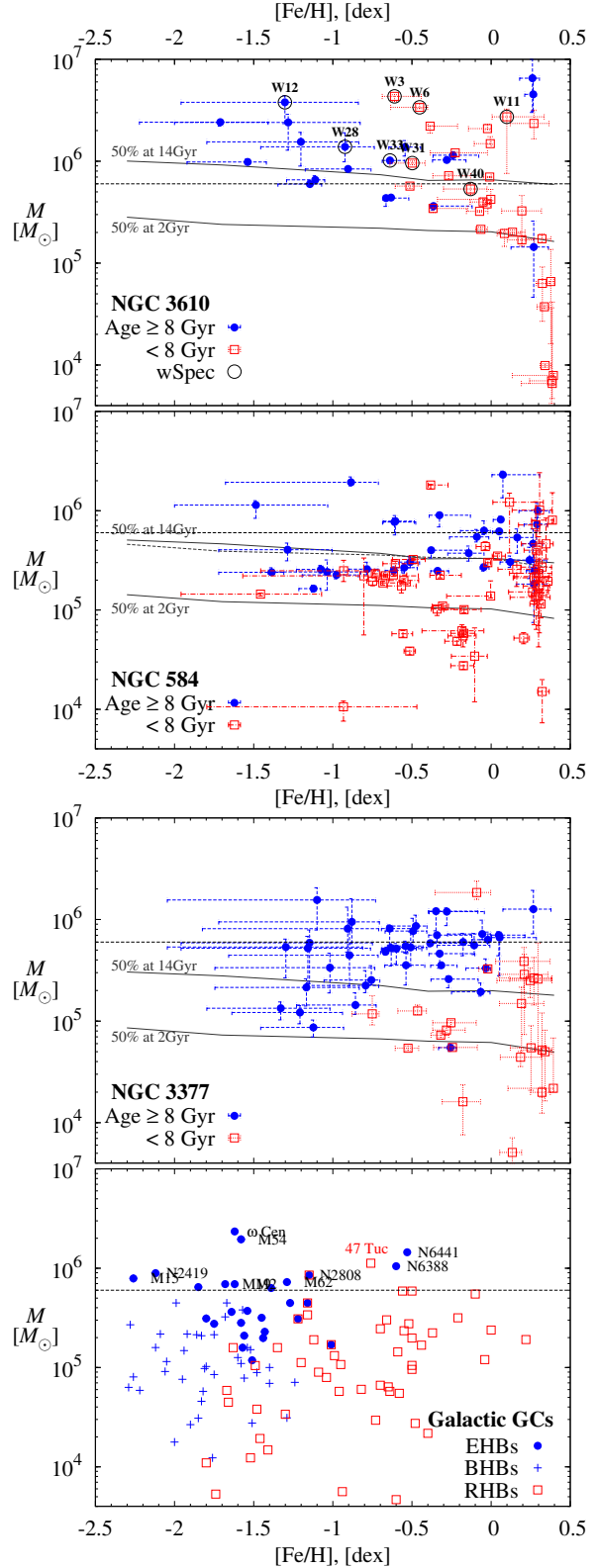


Figure 9. Mass-metallicity distributions for GCs in NGC 3610, NGC 584, NGC 3377 and in the MW (from top to bottom). Solid circles and open squares in the sample galaxies panels show GCs older and younger than 8 Gyr, respectively. Solid symbols, crosses and open squares in the Galactic GCs panel separates GCs with very extended, blue and red horizontal branches. Dashed horizontal line marks the $6 \times 10^5 M_{\odot}$, above which all Galactic GCs except 47 Tuc have BHBs. Labeled solid lines indicate the 50% completeness level at 2 and 14 Gyr.

developed BHBs, which would explain the consistent photometric and spectroscopic ages seen in Figure 4.

7 COMPARING PROPERTIES OF GLOBULAR CLUSTERS WITH THOSE OF THEIR HOST GALAXIES

Our aim is to assess information on the star formation histories (SFHs) of the galaxies in our sample as determined from the properties of their GCs, and compare it to known population properties of the host galaxies themselves. This will not only test for consistency between the two approaches, it will also highlight the particular insights gained from the combination of deep optical and near-IR photometry of GCs in nearby galaxies.

7.1 Ages and metallicities

Under the assumption that massive GCs were formed during major star formation epochs in the galaxies' assembly history, one would expect a relation between the peak ages (and metallicities) for the GCs and the (luminosity-weighted) ages and metallicities of their host galaxies. To test for such a relation, we collected recent age and metallicity measurements for the integrated light of the sample galaxies from the literature. These are listed in Table 6, and were derived from $B-V$ and $B-K$ colours (Li et al. 2007) as well as Lick indices from long-slit spectroscopy by Howell (2005) and Sánchez-Blázquez et al. (2006) using the Thomas et al. (2003) and Vazdekis/MILES SSP models, respectively. Sánchez-Blázquez et al. (2006) provide ages and metallicities from four different index-index diagrams ($[\text{MgbFe}]-\text{H}\beta$, $\text{Fe4383}-\text{H}\beta$, $\text{Mgb}-\text{H}\beta$ and $\text{CN}_2-\text{H}\beta$) and the average of their "best nine spectral synthesis model fits" (giving the oldest age). We selected the average value of all these five measurements, adding errors in quadrature.

For NGC 3377 there are also age and metallicity estimates from the SAURON project (Kuntschner et al. 2010) at R_e , which are $8.1^{+0.4}_{-1}$ Gyr and $[\text{Z}/\text{H}] = -0.23 \pm 0.04$ dex. These were derived from comparing Mgb, Fe50, Fe52, and $\text{H}\beta$ Lick indices to the Vazdekis/MILES SSP models. These values are similar to the results of Sánchez-Blázquez et al. (2006) for NGC 3377. The SAURON values are not included in Table 6 because the other two galaxies were not in the SAURON survey. An interesting result on NGC 3377 from the latter survey is that its inner 20 arcsec (~ 0.7 kpc) region features a relatively young stellar population with high metallicity located in a rotating structure with disc-like kinematics (Kuntschner et al. 2010). This further supports the accretion/interaction-driven formation history of NGC 3377.

Probing for a correlation between the luminosity-weighted stellar age and metallicity of the galaxy and its GCs, we plot the peak age and metallicity of the GCs versus host galaxy age and metallicity in Figure 10. It is clear that the peak age of the red (i.e. metal-rich) GCs in all galaxies is indeed correlated with the luminosity-weighted mean ages and metallicity of the host galaxy.

The upper panel of Figure 10 suggests that the (luminosity-weighted) ages of the sample galaxies are typically younger than the mean ages of their bright metal-rich GCs. While this difference is likely due in part to systematic

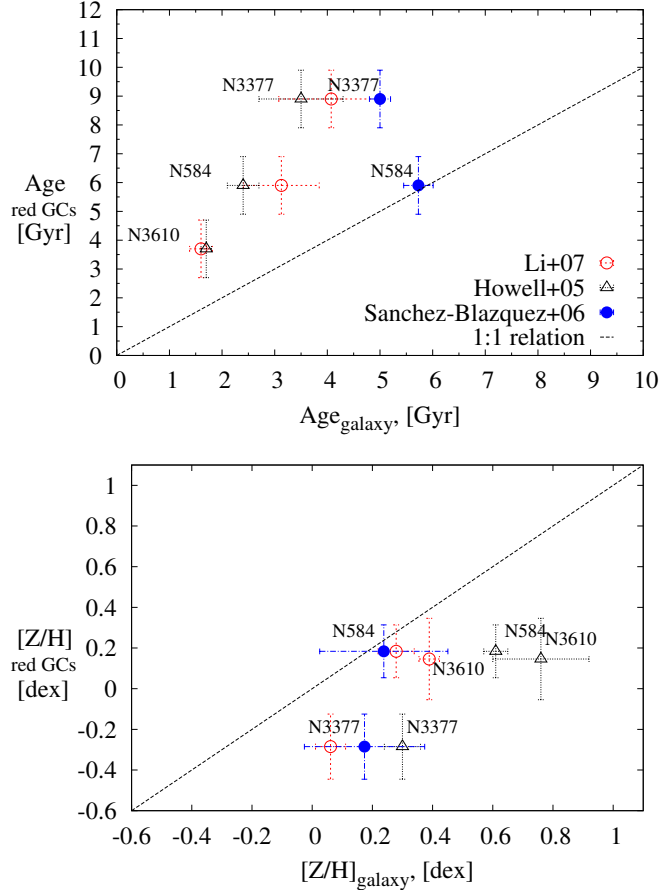


Figure 10. Correlation between ages (top panel) and metallicities (bottom panel) of red globular clusters and integrated light of their host galaxies. Different symbol types represent different literature sources for the (luminosity-weighted) mean age and metallicity of the galaxy, as indicated in the legend. Dashed line is the one-to-one relation.

effects related to the use of different SSP models, this suggests, at face value, that the galaxies had a prolonged star formation history since the major epoch(s) of massive GC formation. One scenario that could cause this effect is that the star formation occurring more recently than the era indicated by the peak age of the metal-rich GCs featured lower star formation rates. This would form fewer high-mass GCs and thus cause fewer GC detections at a given detection threshold, while still causing higher surface brightness for the integrated galaxy light, thus yielding younger ages for the latter. This scenario can be tested directly by probing less massive red GCs with deeper near-IR imaging data in the future, e.g. using the NIRCAM instrument on the James Webb Space Telescope.

7.2 Reconstructing galaxy SFH through its most massive GC

Following recent development on the relation between galaxy star formation rate (SFR) and the luminosity of its most massive cluster at a given epoch, we attempt to derive the galaxy star formation history (SFH) in this section.

The formation efficiency of young massive clusters that can form in a galaxy has been shown to scale with the galaxy

Table 6. Literature values of the age and metallicity of the galaxies in our sample derived from $B - V, B - K$ colours (Li et al. 2007) (columns 2 and 3), and from integrated light spectroscopy based on Lick indices by Howell (2005) based on Thomas et al. (2003) SSPs (columns 4 and 5) and by Sánchez-Blázquez et al. (2006) using Vazdekis/MILES SSPs (columns 6 and 7). In columns 8 and 9 we show the peak age and metallicity of the metal-rich GC subpopulation.

Galaxy	Age [Gyr]	[Z/H]	Age	[Z/H]	Age	[Z/H]	GCs Age	[Z/H]
	from (Li et al. 2007)		(Howell 2005)		(Sánchez-Blázquez et al. 2006)		from this study	
(1)	(2)	(3)	(4)	(5)	(6)	(7)	(8)	(9)
NGC 3610	1.60 ± 0.22	0.389 ± 0.034	1.7 ± 0.1	0.76 ± 0.16	4 ± 1	0.02 ± 0.15
NGC 584	3.13 ± 0.72	0.279 ± 0.060	2.4 ± 0.3	0.61 ± 0.04	6.2 ± 0.69	0.125 ± 0.031	6 ± 1	0.19 ± 0.13
NGC 3377	4.08 ± 1.00	0.061 ± 0.050	3.5 ± 0.8	0.30 ± 0.06	8.9 ± 1.58	-0.010 ± 0.068	9 ± 1	-0.28 ± 0.16

SFR (Larsen & Richtler 2000). Since the SFR is higher for higher gas densities (Kennicutt 1998), the formation of massive clusters becomes more likely as well (Larsen & Richtler 2000; Elmegreen & Efremov 1997). However, the formation of a massive cluster can also be subject to statistical fluctuation resulting from a size-of-sample effect in which higher SFR galaxies will form more GCs and thus sample better the high-mass end of the cluster mass function (Billett et al. 2002; Larsen 2002). Under the assumption that the observed relation between the brightest cluster and the galaxy SFR (Larsen 2002) is explained by a physical limit for the possible range of cluster masses regulated by the galaxy SFR, Weidner et al. (2004) derived relations between the galaxy SFR and the initial (embedded) mass of its most luminous cluster, which allows one to recover the galaxy SFR. To obtain correctly the galaxy SFH, the present-day cluster mass has to be corrected for stellar evolution and dynamical mass-loss to obtain the mass of the cluster at the time of its formation (Maschberger & Kroupa 2007). However, the most luminous cluster in a galaxy is not always the most massive one. For starburst galaxies, the most massive cluster is typically young as shown in Monte Carlo simulations by Bastian (2008). Conversely, if the duration of the Monte Carlo experiment is extended to few Gyr, the oldest clusters are usually the brightest (Gieles 2009). Nevertheless, Bastian (2008) concludes from his Monte Carlo simulations that the observed relation between galaxy SFR and its brightest cluster accurately reflects the recent SFR. Thus, Bastian employs the $M_V^{\text{brightest}}$ vs. SFR relation from Weidner et al. (2004) and corrects for stellar evolution, but not for dynamical mass loss (expected to be small for massive clusters, since the tidal/dynamical mass-loss is inversely proportional to cluster mass; Baumgardt & Makino 2003), the masses of the brightest GCs associated with a given epoch for a sample of major merger galaxies to derive their SFHs. Among the sample of their galaxies is NGC 3610 for which they used the M_V magnitudes from Whitmore et al. (2002) and derived a peak SFR of $218 M_\odot \text{ yr}^{-1}$. Here, we follow the same approach to assess the SFH of the galaxies in our sample as follows.

Using the photometric masses of our clusters, we select the five most massive GC in red three age bins, as shown by vertical dashed lines and indicated with arrows in Figure 11. As several studies have shown that metal-poor GCs and metal-rich GCs trace different components of early-type galaxies, i.e., the halo and bulge/spheroidal components, respectively (e.g., Kissler-Patig et al. 1997; Kundu & Whitmore 1998; Goudfrooij et al. 2007), we distinguish between the metal-poor and metal-rich GCs using $I - K' = 1.4$ as

a dividing colour as before (cf. Section 5.3). The mass of the most massive GCs in those age bins is then used to calculate the galaxy SFR using Eq. 7 of Weidner et al. (2004). To correct the mass of the GCs for mass-loss due to stellar evolution, we used predictions from the Bruzual & Charlot (2003) SSP models. We used the SSP M/L_V at 10 Myr to estimate the clusters' initial masses, as in Bastian (2008). In Figure 12 we show the derived galaxy SFRs from the five most massive GC in three age bins ($t < 4$ Gyr, $t < 8$ Gyr, and $t > 8$ Gyr), where their age positions in the figure are centered around the midpoint of the respective age bin. The peak SFR we derive for NGC 3610 ($234 M_\odot/\text{yr}$) is consistent with the $218 M_\odot/\text{yr}$ derived by Bastian (2008), taking the difference in assumed distance moduli into account they adopt to NGC 3610 from Whitmore et al. (2002) ($\Delta(m - M) = 0.32 \text{ mag}$), as well as the adopted by them solar metallicity for the most massive GC. For the three sample galaxies, Figure 12 shows that the peak star formation was reached at the epoch of formation of the oldest, metal-poor GCs. Since then, dissipative, gas-rich episodic (merger/accretion) events triggered the formation of the younger and more metal-rich stellar populations.

Similarly, we calculate the SFRs of the Milky Way and M 31 from their five most massive old ($t > 8$ Gyr) GCs (cf. Figs. 5 and 11), which are representative for the SFRs at the time of assembly of their spheroid components (bulge and halo). We believe this yields a useful depiction of the uncertainties involved with the use of the most massive GC as a probe of the SFRs within these age bins. We do not expect observational bias effects in the SFR-values due to incompleteness (all measured "brightest" GCs are above the 90% completeness level, see Fig. 11), however we can not exclude the possibility of missing a massive GC which might be located outside of the NIRI and HST WFPC2 or ACS fields (cf. Fig. 1). Effects on the SFRs due to statistical fluctuations in GC mass distribution (Maschberger & Kroupa 2007; Kruijssen & Cooper 2011) must be also kept in mind.

The result of our analysis supports the application of the most massive GCs being a good tracer of the galaxy SFH.

8 CONCLUSIONS

We use new Gemini/NIRI K' -band imaging in conjunction with existing optical V, I HST/WFPC2 and ACS photometry of bright GCs in NGC 3610, NGC 584 and NGC 3377 three early-type galaxies that feature signs of recent galaxy interactions. The addition of the $I - K$ colour effectively breaks the age-metallicity degeneracy present in the $V - I$

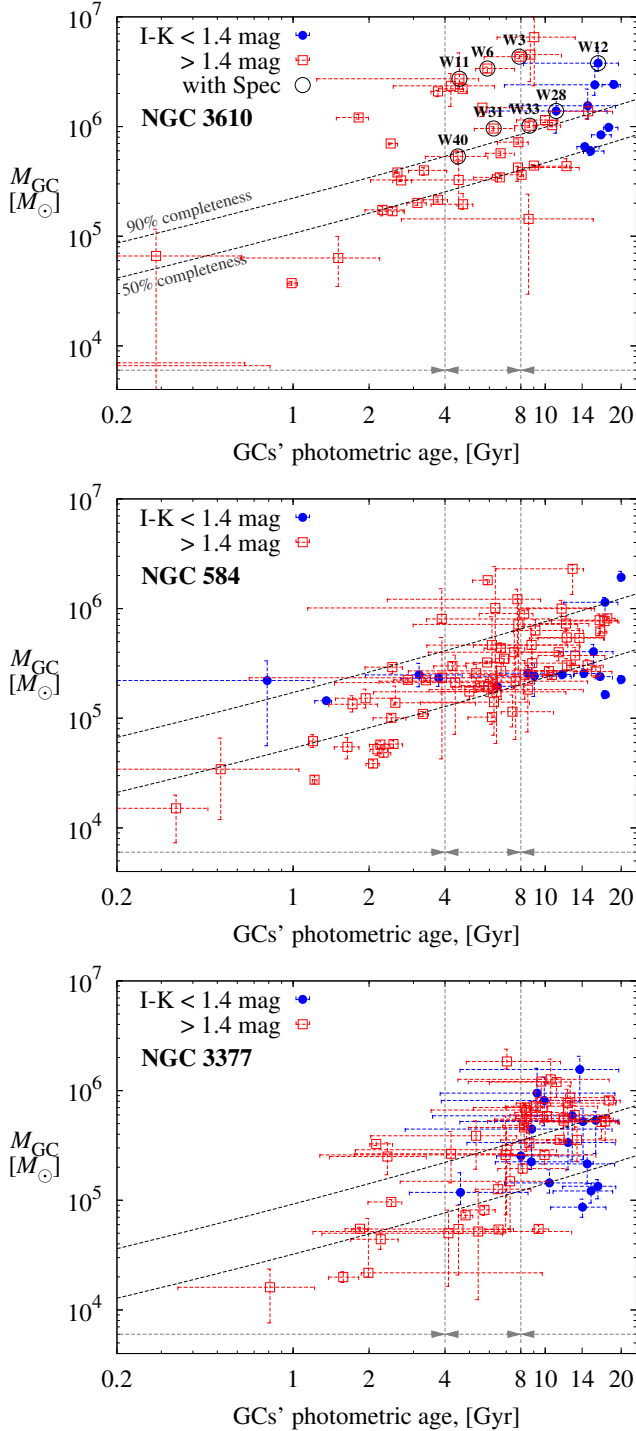


Figure 11. Mass as a function of age for the GCs in NGC 3610, 584 and 3377 from top to bottom. Solid and open symbols indicate clusters bluer or redder than $I-K = 1.4$ mag, i.e. metal-poor or metal-rich. Vertical dashed lines show the age bins within which the most massive GCs were selected to calculate the galaxy SFRs shown in Fig. 12. Dashed curves show the 50% and 90% completeness levels estimated from the SSP models for all metallicities.

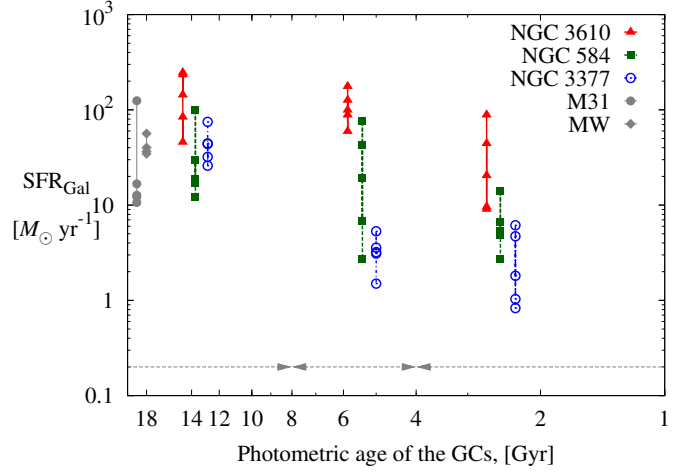


Figure 12. Galaxy star formation rates calculated from the five most massive GCs (symbols connected with lines) in an age bin indicated with arrows at the bottom. The age positions for each galaxy are centered around the midpoint of the age bin, slightly offset from one another to improve visibility. For comparison we show the SFRs of the Milky Way and M31, calculated from their five most massive old GCs, which would be representative for the SFRs of their bulge and spheroid components.

colour. We interpolate between Bruzual & Charlot (2003) SSP model tracks to derive photometric ages, metallicities and masses for all GCs in the sample galaxies. For the massive GCs ($\mathcal{M} \geq 6 \times 10^5 M_{\odot}$) in NGC 3610 with available spectroscopic Lick indices measurements from the literature (Strader et al. 2003, 2004), we find that the photometric ages are older by ~ 2 Gyr. This age difference is larger for the metal-poor GCs, while the photometric and spectroscopic metallicities are in excellent agreement (Sect. 5.1). We argue that this is most likely due to the presence of hot blue HB stars: A comparison with HB properties of Galactic GCs shows that *all* Galactic GCs with $\mathcal{M} \geq 6 \times 10^5 M_{\odot}$ have blue HBs, except the metal-rich GC 47 Tuc. This suggests that all NGC 3610 GCs with spectroscopy found to be older than ~ 8 Gyr are most likely to possess a blue HB as well as the majority of metal-poor GCs with $\mathcal{M} \gtrsim 6 \times 10^5 M_{\odot}$ (in *any* galaxy).

We show that the peak value of the age and metallicity distributions of the sample galaxies GCs is correlated with the luminosity-weighted mean age and metallicity of the host galaxy. The GCs' age and Z distributions are broad (Sect. 5.3), indicating a prolonged star and cluster formation history. We reconstruct the galaxies' SFHs from the GC age distributions, using the recently observed correlation between the luminosity of the most massive GC at a given age and the galaxy SFR (Sect. 7.2).

Our results support a scenario in which the star formation rate of the three candidate intermediate-age galaxies in our sample peaked at the epoch at which the oldest GCs (i.e., the metal-poor ones) formed. Subsequent dissipative events (i.e., interactions involving gas-rich galaxies) led to the formation of more metal-rich GCs up to a few Gyr ago. The SFHs of our sample galaxies as determined from their GCs suggests that the SFR was highest at the earliest times ($\gtrsim 10$ Gyr ago in all three cases. The latter is in large part due to the presence of massive metal-poor

GCs which are likely associated with the early build-up of the galaxy halos. The strengths of subsequent star formation events occurring over the last ~ 10 Gyr varied significantly from one galaxy to another. Among the three galaxies in our sample, NGC 3610 showed the strongest SFR in all age bins, especially at the youngest age bin (< 4 Gyr ago). This is consistent with NGC 3610 being the most luminous galaxy in our sample as well as having the youngest spectroscopically determined age.

The ability to obtain such direct insights on the SFHs of galaxies renders the study of galactic GC systems in the optical vs. near-IR a promising tool to trace galaxy formation, merging and star formation history.

ACKNOWLEDGMENTS

We would like to acknowledge the useful comments by the referee. IG would like to thank Dr. A. Kundu for kindly providing their tables with the HST/WFPC2 photometry of GCs in NGC 3377 and NGC 584. IG is thankful for the received support by the German Research Foundation (Deutsche Forschungsgemeinschaft, DFG) grant DFG - Projekt BO-779/32-1. IYG and PG thank the Director of STScI for funding part of this research through a director's discretionary research grant. The authors would like to acknowledge useful discussions with Prof. P. Kroupa. This paper is based on observations obtained at the Gemini Observatory, which is operated by the Association of Universities for Research in Astronomy, Inc., under a cooperative agreement with the NSF on behalf of the Gemini partnership: the National Science Foundation (United States), the Science and Technology Facilities Council (United Kingdom), the National Research Council (Canada), CONICYT (Chile), the Australian Research Council (Australia), Ministério da Ciência e Tecnologia (Brazil) and Ministerio de Ciencia, Tecnología e Innovación Productiva (Argentina).

We acknowledge the usage of the HyperLeda database <http://leda.univ-lyon1.fr> (Paturel et al. 2003). This research has made use of the NASA/IPAC Extragalactic Database (NED) which is operated by the Jet Propulsion Laboratory, California Institute of Technology, under contract with the National Aeronautics and Space Administration.

Facilities: Gemini (NIRI), HST (ACS, WFPC2).

REFERENCES

- Alves-Brito A., Hau G. K. T., Forbes D. A., Spitler L. R., Strader J., Brodie J. P., Rhode K. L., 2011, *MNRAS*, pp 1306–+
- Anders P., Fritze-v. Alvensleben U., 2003, *A&A*, 401, 1063
- Anders P., Lamers H. J. G. L. M., Baumgardt H., 2009, *A&A*, 502, 817
- Ashman K. M., Zepf S. E., 1992, *ApJ*, 384, 50
- Barmby P., Huchra J. P., Brodie J. P., 2001, *AJ*, 121, 1482
- Barmby P., Huchra J. P., Brodie J. P., Forbes D. A., Schroder L. L., Grillmair C. J., 2000, *AJ*, 119, 727
- Barmby P., McLaughlin D. E., Harris W. E., Harris G. L. H., Forbes D. A., 2007, *AJ*, 133, 2764
- Bastian N., 2008, *MNRAS*, 390, 759
- Baumgardt H., Makino J., 2003, *MNRAS*, 340, 227
- Beasley M. A., Brodie J. P., Strader J., Forbes D. A., Proctor R. N., Barmby P., Huchra J. P., 2005, *AJ*, 129, 1412
- Billett O. H., Hunter D. A., Elmegreen B. G., 2002, *AJ*, 123, 1454
- Brocato E., Castellani V., Poli F. M., Raimondo G., 2000, *A&As*, 146, 91
- Brodie J. P., Strader J., Denicoló G., Beasley M. A., Cenarro A. J., Larsen S. S., Kuntschner H., Forbes D. A., 2005, *AJ*, 129, 2643
- Bruzual G., Charlot S., 2003, *MNRAS*, 344, 1000
- Caldwell N., Schiavon R., Morrison H., Rose J. A., Harding P., 2011, *AJ*, 141, 61
- Cantiello M., Blakeslee J., Raimondo G., Brocato E., Capaccioli M., 2007, *ApJ*, 668, 130
- Cantiello M., Blakeslee J. P., 2007, *ApJ*, 669, 982
- Carlsberg Meridian Catalogue ed. 1989, Carlsberg Meridian Catalogue La Palma. Number 4: Observations of positions of stars and planets: May 1984 to February 1988
- Servicio Publicaciones Armada, Copenhagen University Observatory, Royal Greenwich Observatory and Real Instituto y Observatorio de la Armada en San Fernando
- Carretta E., Bragaglia A., Gratton R. G., Recio-Blanco A., Lucatello S., D'Orazi V., Cassisi S., 2010, *A&A*, 516, A55+
- Cenarro A. J., Beasley M. A., Strader J., Brodie J. P., Forbes D. A., 2007, *AJ*, 134, 391
- Chabrier G., 2003, *PASP*, 115, 763
- Chies-Santos A. L., Larsen S. S., Kuntschner H., Anders P., Wehner E. M., Strader J., Brodie J. P., Santos J. F. C., 2011, *A&A*, 525, A20+
- de Vaucouleurs G., de Vaucouleurs A., Corwin Jr. H. G., Buta R. J., Paturel G., Fouque P., 1991, *Third Reference Catalogue of Bright Galaxies*
- Dotter A., Sarajedini A., Anderson J., 2011, *ApJ*, 738, 74
- Dotter A., Sarajedini A., Anderson J., Aparicio A., Bedin L. R., Chaboyer B., Majewski S., Marín-Franch A., Milone A., Paust N., Piotto G., Reid I. N., Rosenberg A., Siegel M., 2010, *ApJ*, 708, 698
- Elmegreen B. G., Efremov Y. N., 1997, *ApJ*, 480, 235
- Forbes D. A., Georgakakis A. E., Brodie J. P., 2001, *MNRAS*, 325, 1431
- Georgiev I. Y., Hilker M., Puzia T. H., Goudfrooij P., Baumgardt H., 2009, *MNRAS*, 396, 1075
- Gieles M., 2009, *Ap&SS*, 324, 299
- Goudfrooij P., Alonso M. V., Maraston C., Minniti D., 2001, *MNRAS*, 328, 237
- Goudfrooij P., Mack J., Kissler-Patig M., Meylan G., Minniti D., 2001, *MNRAS*, 322, 643
- Goudfrooij P., Schweizer F., Gilmore D., Whitmore B. C., 2007, *AJ*, 133, 2737
- Harris W. E., 1996, *AJ*, 112, 1487
- Harris W. E., Harris G. L. H., Layden A. C., Stetson P. B., 2007, *AJ*, 134, 43
- Hawarden T. G., Leggett S. K., Letawsky M. B., Ballantyne D. R., Casali M. M., 2001, *MNRAS*, 325, 563
- Hempel M., Kissler-Patig M., Puzia T. H., Hilker M., 2007, *A&A*, 463, 493
- Hempel M., Zepf S., Kundu A., Geisler D., Maccarone T. J., 2007, *ApJ*, 661, 768
- Hodapp K. W., Jensen J. B., Irwin E. M., Yamada H., Chung R., Fletcher K., Robertson L., Hora J. L., Simons D. A., Mays W., Nolan R., Bec M., Merrill M., Fowler

- A. M., 2003, *PASP*, 115, 1388
- Holtzman J. A., Faber S. M., Shaya E. J., Lauer T. R., Groth J., Hunter D. A., Baum W. A., Ewald S. P., Hester J. J., Light R. M., Lynds C. R., O'Neil Jr. E. J., Westphal J. A., 1992, *AJ*, 103, 691
- Howell J. H., 2005, *AJ*, 130, 2065
- Kennicutt Jr. R. C., 1998, *ApJ*, 498, 541
- Kissler-Patig M., Forbes D. A., Minniti D., 1998, *MNRAS*, 298, 1123
- Kissler-Patig M., Kohle S., Hilker M., Richtler T., Infante L., Quintana H., 1997, *A&A*, 319, 470
- Koleva M., Prugniel P., Ocvirk P., Le Borgne D., Soubiran C., 2008, *MNRAS*, 385, 1998
- Kroupa P., 2001, *MNRAS*, 322, 231
- Kruijssen J. M. D., Cooper A. P., 2011, *ArXiv:1110.4106*
- Kundu A., Whitmore B. C., 1998, *AJ*, 116, 2841
- Kundu A., Whitmore B. C., 2001, *AJ*, 121, 2950
- Kundu A., Zepf S. E., 2007, *ApJL*, 660, L109
- Kundu A., Zepf S. E., Hempel M., Morton D., Ashman K. M., Maccarone T. J., Kissler-Patig M., Puzia T. H., Vesperini E., 2005, *ApJL*, 634, L41
- Kuntschner H., Emsellem E., Bacon R., Cappellari M., Davies R. L., de Zeeuw P. T., Falcón-Barroso J., Krajnović D., McDermid R. M., Peletier R. F., Sarzi M., Shapiro K. L., van den Bosch R. C. E., van de Ven G., 2010, *MNRAS*, 408, 97
- Kuntschner H., Ziegler B. L., Sharples R. M., Worthey G., Fricke K. J., 2002, *A&A*, 395, 761
- Landolt A. U., 1992, *AJ*, 104, 340
- Larsen S. S., 2002, *AJ*, 124, 1393
- Larsen S. S., Brodie J. P., Beasley M. A., Forbes D. A., Kissler-Patig M., Kuntschner H., Puzia T. H., 2003, *ApJ*, 585, 767
- Larsen S. S., Brodie J. P., Huchra J. P., Forbes D. A., Grillmair C. J., 2001, *AJ*, 121, 2974
- Larsen S. S., Richtler T., 2000, *A&A*, 354, 836
- Lasker B. M., Sturch C. R., Lopez C., Mallamas A. D., McLaughlin S. F., Russell J. L., Wisniewski W. Z., Gillespie B. A., Jenkner H., Siciliano E. D., Kenny D., Baumert J. H., Goldberg A. M., Henry G. W., Kemper E., Siegel M. J., 1988, *ApJs*, 68, 1
- Lee H.-c., Yoon S.-J., Lee Y.-W., 2000, *AJ*, 120, 998
- Lee Y.-W., Gim H. B., Casetti-Dinescu D. I., 2007, *ApJL*, 661, L49
- Leggett S. K., 1992, *ApJs*, 82, 351
- Leggett S. K., Currie M. J., Varricatt W. P., Hawarden T. G., Adamson A. J., Buckle J., Carroll T., Davies J. K., Davis C. J., Kerr T. H., Kuhn O. P., Seigar M. S., Wold T., 2006, *MNRAS*, 373, 781
- Li Z., Han Z., Zhang F., 2007, *A&A*, 464, 853
- Maraston C., 2005, *MNRAS*, 362, 799
- Maschberger T., Kroupa P., 2007, *MNRAS*, 379, 34
- Masters K. L., Jordán A., Côté P., Ferrarese L., Blakeslee J. P., Infante L., Peng E. W., Mei S., West M. J., 2010, *ApJ*, 715, 1419
- McCook G. P., Sion E. M., 1987, *ApJs*, 65, 603
- McLaughlin D. E., van der Marel R. P., 2005, *ApJS*, 161, 304
- Michard R., 2005, *A&A*, 441, 451
- Miller B. W., Whitmore B. C., Schweizer F., Fall S. M., 1997, *AJ*, 114, 2381
- Ocvirk P., 2010, *ApJ*, 709, 88
- Paturel G., Petit C., Prugniel P., Theureau G., Rousseau J., Brouty M., Dubois P., Cambrésy L., 2003, *A&A*, 412, 45
- Peng E. W., Jordán A., Côté P., Blakeslee J. P., Ferrarese L., Mei S., West M. J., Merritt D., Milosavljević M., Tonry J. L., 2006, *ApJ*, 639, 95
- Percival S. M., Salaris M., 2011, *MNRAS*, 412, 2445
- Perina S., Galletti S., Fusi Pecci F., Bellazzini M., Federici L., Buzzoni A., 2011, *ArXiv e-prints*
- Puzia T. H., Kissler-Patig M., Thomas D., Maraston C., Saglia R. P., Bender R., Goudfrooij P., Hempel M., 2005, *A&A*, 439, 997
- Puzia T. H., Saglia R. P., Kissler-Patig M., Maraston C., Greggio L., Renzini A., Ortolani S., 2002, *A&A*, 395, 45
- Puzia T. H., Zepf S. E., Kissler-Patig M., Hilker M., Minniti D., Goudfrooij P., 2002, *A&A*, 391, 453
- Raimondo G., Brocato E., Cantiello M., Capaccioli M., 2005, *AJ*, 130, 2625
- Recio-Blanco A., Aparicio A., Piotto G., de Angeli F., Djorgovski S. G., 2006, *A&A*, 452, 875
- Sánchez-Blázquez P., Gorgas J., Cardiel N., González J. J., 2006, *A&A*, 457, 809
- Sandage A., Katem B., 1982, *AJ*, 87, 537
- Sandage A., Tammann G. A., 1981, *A revised Shapley-Ames Catalog of bright galaxies*. Washington: Carnegie Institution, 1981
- Schiavon R. P., Rose J. A., Courteau S., MacArthur L. A., 2004, *ApJL*, 608, L33
- Schlegel D. J., Finkbeiner D. P., Davis M., 1998, *ApJ*, 500, 525
- Schweizer F., 1987, *Star formation in colliding and merging galaxies*. Springer: New York, pp p.18–25
- Schweizer F., Miller B. W., Whitmore B. C., Fall S. M., 1996, *AJ*, 112, 1839
- Spitler L. R., Forbes D. A., Beasley M. A., 2008, *MNRAS*, 389, 1150
- Strader J., Brodie J. P., Forbes D. A., 2004, *AJ*, 127, 295
- Strader J., Brodie J. P., Schweizer F., Larsen S. S., Seitzer P., 2003, *AJ*, 125, 626
- Thomas D., Maraston C., Bender R., 2003, *MNRAS*, 339, 897
- Tokunaga A. T., Simons D. A., Vacca W. D., 2002, *PASP*, 114, 180
- Tonry J. L., Dressler A., Blakeslee J. P., Ajhar E. A., Fletcher A. B., Luppino G. A., Metzger M. R., Moore C. B., 2001, *ApJ*, 546, 681
- Trager S. C., Faber S. M., Worthey G., González J. J., 2000, *AJ*, 120, 165
- Vazdekis A., Sánchez-Blázquez P., Falcón-Barroso J., Cenarro A. J., Beasley M. A., Cardiel N., Gorgas J., Peletier R. F., 2010, *MNRAS*, 404, 1639
- Weidner C., Kroupa P., Larsen S. S., 2004, *MNRAS*, 350, 1503
- Whitmore B. C., Schweizer F., Kundu A., Miller B. W., 2002, *AJ*, 124, 147
- Whitmore B. C., Zhang Q., Leitherer C., Fall S. M., Schweizer F., Miller B. W., 1999, *AJ*, 118, 1551
- Woodley K. A., Harris W. E., Puzia T. H., Gómez M., Harris G. L. H., Geisler D., 2010, *ApJ*, 708, 1335
- Worthey G., 1994, *ApJs*, 95, 107
- Worthey G., Faber S. M., Gonzalez J. J., Burstein D., 1994, *ApJS*, 94, 687

- Xin Y., Deng L., de Grijs R., Kroupa P., 2011, MNRAS,
411, 761
Yi S. K., 2003, ApJ, 582, 202
Yoon S., Yi S. K., Lee Y., 2006, Science, 311, 1129